Invariant neural responses for sensory categories revealed by the time-varying information for communication calls

Julie E. Elie[1,2*] and Frédéric E. Theunissen[1,3].

1. Helen Wills Neuroscience Institute. University of California, Berkeley.
2. Department of Bioengineering. University of California, Berkeley.
3. Department of Psychology. University of California, Berkeley.

*Corresponding Author:

julie.elie@berkeley.edu

Short Title: Time-varying information for auditory objects.

Abstract.

Although information theoretic approaches have been used extensively in the analysis of the neural code, they have yet to be used to describe how information is accumulated in time while sensory systems are categorizing dynamic sensory stimuli such as speech sounds or visual objects. Here, we present a novel method to estimate the cumulative information for stimuli or categories. We further define a time-varying categorical information index that, by comparing the information obtained for stimuli versus categories of these same stimuli, quantifies invariant neural representations. We use these methods to investigate the dynamic properties of avian cortical auditory neurons recorded in zebra finches that were listening to a large set of call stimuli sampled from the complete vocal repertoire of this species. We found that the time-varying rates carry 5 times more information than the mean firing rates even in the first 100 *ms*. We also found that cumulative information has slow time constants (100-600 *ms*) relative to the typical integration time of single neurons, reflecting the fact that the behaviorally informative features of auditory objects are time-varying sound patterns. When we correlated firing rates and information values, we found that average information correlates with average firing rate but that higher-rates found at the onset response yielded similar information values as the lower-rates found in the sustained response: the onset and sustained response of avian cortical auditory neurons provide similar levels of independent information about call identity and call type. Finally, our information measures allowed us to rigorously define categorical neurons; these categorical neurons show a high degree of invariance for vocalizations within a call-type. Surprisingly, call-type invariant neurons were found in both primary and secondary avian auditory areas.

Author Summary

Just as the recognition of faces requires neural representations that are invariant to scale and rotation, the recognition of behaviorally relevant auditory objects, such as spoken words, requires neural representations that are invariant to the speaker uttering the word and to his or her location. Here, we used information theory to investigate the time course of the neural representation of bird communication calls and of behaviorally relevant categories of these same calls: the call-types of the bird's repertoire. We found that neurons in both the primary and secondary avian auditory cortex exhibit invariant responses to call renditions within a call-type, suggestive of a potential role for extracting the meaning of these communication calls. We also found that time plays an important role: first, neural responses carry significant more information when represented by temporal patterns calculated at the small time scale of 10 ms than when measured as average rates and, second, this information accumulates in a non-redundant fashion up to long integration times of 600 ms. This rich temporal neural representation is matched to the temporal richness found in the communication calls of this species.

Introduction

Information theoretic analyses are well suited to the study of neural representation since this mathematical framework was developed to quantify and optimize the encoding of informative signals in communication channels [1]. In sensory systems, Information Theory (IT) has been applied extensively as a complimentary approach to the estimation of stimulus-response functions such as tuning curves, spatio-temporal or spectro-temporal receptive fields or other higher-level encoding models [2]. Information theoretic approaches have been particularly powerful in explorations of the nature of the neural code and its redundancy or efficiency [3-6]. For example, IT was used in early studies in the visual system to

demonstrate that spike patterns contain information beyond average rate both for static images [7] and dynamic visual stimuli [8]. IT was also used to show that spike doublets can contain synergistic information that cannot be explained by an analysis of successive single spikes [9] and that, although information can only decrease in a signal processing chain, the neural coding efficiency increases as one moves to higher levels of sensory processing [10]. Finally, IT investigations also revealed that neural efficiency is higher when sensory systems process natural stimuli versus synthetic stimuli [11-13], in support of ethological theories of optimal sensory processing [14].

In sensory systems, the mutual information between a stimulus and the neural responses has often been estimated in a stimulus reconstruction framework and for continuous dynamic stimuli in stationary conditions, where time averages can be performed. In the stimulus reconstruction framework, one attempts to estimate the information about all aspects of the stimulus; for example, in audition, the stimulus would be represented by its exact sound pressure waveform. As long as the stimulus set is rich (i.e. has very large entropy), the mutual information can be an estimate of the maximum information that can be transmitted by a neural communication channel, also known as the channel capacity [3, 4]. For instance, one can obtain the mutual information of an adapted auditory neuron processing white noise or colored noise sounds [11]. As long as the stationary assumption is valid, using continuous stimuli is also beneficial as it provides large data sets that are needed to estimate the joint probability of stimuli and neural responses, both of which can have high dimensions. Even in these conditions, it is noteworthy that a direct estimation of information is only possible when many repeats of the same stimulus can be obtained [15] or when simplifying assumptions are made [9]. Ultimately, the calculation of information based on stimulus reconstruction gives a single number corresponding to the information transmitted by a single neuron or an ensemble of neurons for a particular stimulus ensemble. By repeating the

calculation for different stimulus ensembles, one can investigate how the channel capacity of particular neurons or neural ensembles might depend on the stimulus statistics (e.g. for natural vs synthetic stimuli). Furthermore, by repeating the calculation using different symbols to represent the response, the potential nature of the neural code (e.g. time patterns vs. rate) can be revealed.

Here we are using IT in a different sensory encoding context: the accumulation of information in a recognition task, such as face recognition in the visual system [16] or word recognition in the auditory system [17]. Recognition or identification is one of the key computations performed by higher sensory areas as opposed to the task of efficient stimulus representations that is performed in lower sensory areas and that might therefore be well quantified by information values based on stimulus reconstruction. In the recognition tasks, each stimulus is described by a simple label, such as the word corresponding to a given speech sound or that is used to label a given visual object. The relevant value of information in that task is then the information about these discrete labels and the information capacity of the system in its ability to identify the stimulus as a whole. In the recognition framework, one can ask how the information about the stimulus identity or label changes as a function of time relative to the stimulus onset and to what extent that time-varying information is redundant and, thus, how it accumulates over time. For example, one could ask at what time after stimulus onset does the performance of single neurons or ensemble of neurons match a behavioral performance of word recognition. Such an IT analysis has been performed in the primate visual system using a delay-matching to sample paradigm, and using spike counts, estimated in progressively longer windows, as the neural symbols [18].

In information studies based on continuous stimulus reconstruction, the neural code can be investigated in terms of its temporal resolution (i.e. letter size) and its integration time (i.e. word length). While the same properties of the neural code can be deciphered in the

114 recognition framework, one can also examine the relationship between spikes at different
115 points in time and time-varying information. This analysis is meaningful because a time zero
116 corresponding to stimulus onset can be clearly defined and is behaviorally relevant.
117 Moreover, stimulus-response functions for such discrete stimuli are not time-invariant.
118 Responses in sensory neurons, in vision [19, 20] and in audition [21, 22], are often
119 characterized by an onset response (or on-response) and a sustained response, where both the
120 precision of spikes and the information coded might be different [23, 24]. For example, a first
121 spike latency code has been proposed as a fast encoding scheme in vision [25], audition [26]
122 and somato-sensation [27]. Rolls et al. tested this hypothesis, by quantifying the fraction of
123 information that is present in the first spike relative the on-going response [28].
124 Finally, in the recognition framework, one can also compare the information values
125 obtained when different labelling schemes are used for identifying the stimuli as objects. For
126 example, speech sounds could be labeled hierarchically as unique utterances, as phonemes, as
127 syllables, as words, etc.. One can then compare time-varying information about each of the
128 levels in such hierarchical labelling scheme and gain insight on the neuro processing involved
129 in object categorization. Although such a hierarchical representation of stimulus features has
130 been used in encoding models for studying human processing [29], it has not yet been used in
131 an IT analysis.
132 In this study, we developed a new approach for estimating time-varying information
133 and cumulative information for sensory object identification task. Our approach assumes that
134 time-varying neural responses can be modeled as inhomogeneous Poisson processes and
135 generalizes well to large number of stimulus categories and to long integration times relative
136 to the dynamics of the time-varying response. Our motivation for developing this
137 methodology was to gain additional understanding on the neural representation of
138 communication signals in high level auditory areas. Animal communication calls, just as

139 speech sounds in humans, are categorized into behaviorally meaningful units. Significant
140 progress has been made in identifying brain regions involved in categorizing sounds, in
141 particular in the primate brain, where neural responses that are correlated with progressively
142 more abstracts concepts are found in primary auditory cortex, the lateral belt of the auditory
143 cortex and the prefrontal cortex [30]. However, the neural computations involved in
144 generating categorical responses remain poorly described [31] and only a small number of
145 studies have examined the neural categorization of natural communication calls in non-
146 human species [32-36]. We and others have been developing an avian model system to study
147 the neural processing of relatively large and complex vocal repertoires [37, 38]. Our prior
148 studies include a detailed bioacoustical analysis of the features that define each call-type of
149 the complete vocal repertoire of the zebra finch [39] and the first characterization of neural
150 responses to the calls from that large repertoire in primary and secondary avian auditory
151 cortical areas [40]. In that study, we found that approximately 45% of auditory neurons
152 encode information about call-type categories. Among those, a minority show strong
153 selectivity for single call-type categories and invariance for calls within that category. Here,
154 we investigated the processing in time that could lead to those observed categorical responses
155 by comparing the time-varying information for stimuli labelled as individual utterances to the
156 time-varying information for the same stimuli labelled by their call-type category. With that
157 analysis, we were able to obtain values of temporal integration for stimulus identification and
158 call-type category identification. We also analyzed the relationship between the time-varying
159 firing rate and the time-varying information and, in particular, examined differences in
160 selectivity in the onset versus sustained response. Finally, we used anatomical data to
161 examine the distribution of neurons in primary and secondary avian auditory cortical areas
162 with distinct responses properties as revealed by this IT analysis.
163

Results

We studied the time-varying information in a population of neurons recorded from primary and secondary regions in the avian auditory cortex of head-fixed urethane anesthetized zebra finches listening to a large set of natural communication calls. Zebra finches emit various calls in different behavioral contexts and have a complete vocal repertoire composed of 11 call-types. The acoustical characteristics of each call-type have previously been described in detail [39]. Here we focused on the neural representation of 9 call-types: 1) 3 pro-social calls emitted for pair bonding and social cohesion: the Distance Call (DC), the Tet Call (Te), the Nest Call (Ne); 2) the Song (So) that is emitted as a sexual display in males; 3) 2 calls emitted in aggressive encounters: the aggressive Wsst Call (Ws) and the Distress Call (Di); 4) 1 alarm call, the Thuk Call (Th) and 5) 2 calls emitted by juveniles: the Begging Call (Be), used by young to request food, and the Long Tonal Call (LT), a contact call that is a precursor of the adult DC. A stimulus set was composed of approximately 10 different exemplars of calls, train of calls or song produced by different vocalizers for each of the 9 call-types. The call stimuli were randomly sampled from a large annotated data base of calls and songs from the complete repertoire of the male and female zebra finch. Neural responses were recorded using electrode arrays implanted in both hemispheres of 4 male and 2 female adult zebra finches. We recorded from a total of 914 single auditory units in both primary (Field L) and secondary (CML, CMM and NCM) avian auditory areas. In previous analysis, we showed using a decoding approach that information about call-types was found in 404 (44%) of these units [40]. Here, we further restricted our population analysis of information to neurons, from that same data set, that reached a significant level of information about the stimulus (see methods) and analyzed the time-varying information of 337 neurons during the first 600 ms of their response. Note that many calls are shorter than 600 ms, but also that they are often produced in succession with short

inter-call intervals. Thus, this analysis window could contain two or more calls or the beginning of a longer song motif comprised of multiple syllables. We only analyzed the response in the first 600 ms because the estimation of the cumulative information for longer time windows became unreliable, as we will explain below. Additional details on the neurophysiological recordings can be found in the methods section and in Elie and Theunissen [40].

In the *Results*, we first describe the approach we developed to estimate instantaneous and cumulative time varying information. We illustrate these calculations with specific examples of model and actual neurons in the avian auditory cortex. We then analyze the time-varying coding properties of the avian cortical auditory neurons with an emphasis on: the relationship between spike rate and instantaneous information, the time constants observed for the cumulative information and the relative fraction of stimulus cumulative information that is used for extracting the behaviorally relevant categories corresponding to distinct call-types.

Estimation of the time-varying information

At a given time t, the *instantaneous* mutual information between the stimulus S and the response Y_t can be written as a difference in Shannon entropies:

$$I_t = H(Y_t) - H(Y_t|S)$$

Here, $H(Y_t)$ is the response entropy for a window at time *t*, while $H(Y_t|S)$ corresponds to entropy of the response given the stimulus or the conditional response entropy. $H(Y_t|S)$ can also be called the neural noise since it represents the variability in the neural response to the same stimulus. For spiking neurons, y_t represents the number of spikes in the window at time *t* (Note: In our notation, capitals are used for random variables and lower case for a sample from that random variable).

Similarly, the cumulative mutual information in neural responses that are discretized into time intervals is given by:

$$CI_t = H(Y_t, Y_{t-1}, Y_{t-2}, \ldots, Y_0) - H(Y_t, Y_{t-1}, Y_{t-2}, \ldots, Y_0 \mid S)$$

The entropies now include the time course of the neural responses starting at t=0 and up to time t. The reference time t=0 is set to the stimulus onset in our analyses but could be any arbitrary reference point.

The conditional response entropy and the response entropy are obtained from the distribution of the conditional probability of neural responses given the stimulus, $p(y_t|s)$, and the distribution of probability of each stimulus $p(s_i)$:

$$H(Y_t|S) = \sum_i p(s_i) \sum_{y_t=0}^{R_{Max}} -p(y_t \mid s_i) \log_2 p(y_t \mid s_i)$$

$$H(Y_t) = \sum_{y_t=0}^{R_{Max}} -p(y_t) \log_2 p(y_t)$$

$$\text{with } p(y_t) = \textstyle\sum_i p(s_i) p(y_t|s_i)$$

y_t, the neural response at time t, is measured in spike counts and takes values from zero to a maximum rate value, R_{Max}(for example, as dictated by the neuron's refractory period or numerically as $p \log p$ becomes infinitely small for high spike counts that have very small probability of occurring). The probability of the stimulus $p(s_i)$ is usually taken as $1/n_s$, where n_s is the number of stimuli, unless the study incorporates natural stimulus statistics. The probability of spike counts at time t given a stimulus, $p(y_t|s_i)$, could be estimated empirically by recording hundreds or thousands of responses of the same neuron to the same stimulus. Although this approach has been shown to be possible in certain preparations [15], it severely limits the number of stimuli that can be investigated in most neurophysiological experiments. Here we propose a parametric approach where we model the distribution of

neural responses to a given stimulus s_i as an inhomogeneous Poisson process. The conditional probability of response (spike count) given the stimulus is then:

$$p(y_t|s_i) = \frac{\mu_{s_i}(t)^{y_t}}{y_t!} e^{-\mu_{s_i}(t)}$$

where $\mu_{s_i}(t)$ is the mean response at time *t* for stimulus s_i . This mean rate was estimated empirically using the time varying kernel density estimation (KDE) proposed by Shimazaki and Shinomoto [41]. The instantaneous information estimated in this fashion is relatively straightforward, as long as the Poisson assumption is valid and a sufficient number of trials is obtained to estimate $\mu_{s_i}(t)$ (see methods).

The estimation of the cumulative information then extends this approach to joint probabilities of responses in successive time windows, $(y_t, y_{t-1}, y_{t-2}, \ldots)$. Due to what has been labelled as the "curse of dimensionality", the numerical estimation of the unconditional probability becomes exponentially more expensive as the integration time increases. We evaluated multiple approaches based on different assumptions and found that Monte Carlo with importance sampling yielded the best results (see methods and Sup. Fig. 3 for comparison to alternative approaches).

Given our Poisson assumption, the conditional probability of response at *t* is independent of the conditional response at previous times.

$$p(y_t, y_{t-1}, y_{t-2}, \ldots \mid s_i) = p(y_t \mid s_i) p(y_{t-1} \mid s_i) p(y_{t-2} \mid s_i) \ldots$$

Because of this probabilistic independence, it can be shown that the joint conditional response entropy is simply the sum of the conditional response entropies at each time point (see methods):

$$H(Y_t, Y_{t-1}, Y_{t-2}, \ldots \mid S) = H(Y_t \mid S) + H(Y_{t-1} \mid S) + H(Y_{t-2} \mid S) + \ldots$$

Thus, the estimation of the conditional response entropy is straightforward and not affected by the integration time. The problem of dimensionality arises in the estimation of the unconditional probabilities of response and the corresponding response entropy.

The probability of the time varying response is the joint probability of observing $(y_t, y_{t-1}, y_{t-2}, \ldots)$. This joint probability cannot be expressed as the product of the probabilities at different times because these are not independent. More intuitively observing a particular y_{t-1} will affect the probability of observing y_t. This is true because the time varying means of the Poisson distributions $\mu_{s_i}(t)$ are correlated in time; for example, if $\mu_{s_i}(t-1)$ is high we might expect $\mu_{s_i}(t)$ to also have high values. These high values could be true for one particular stimulus s_i but not for the other stimuli. Then observing a high value of y_{t-1} would predict a higher value than expected for y_t (and an increase in probability that it was caused by s_i). The joint unconditional probability distribution is:

$$p(y_t, y_{t-1}, y_{t-2}, \ldots) = \sum_{s_i} p(s_i)[p(y_t \mid s_i)p(y_{t-1} \mid s_i)p(y_{t-2} \mid s_i)\ldots] \neq p(y_t)p(y_{t-1})p(y_{t-2})\ldots$$

Given the lack of independence, the response entropy must then be calculated from the joint probability distribution:

$$H(Y_t, Y_{t-1}, Y_{t-2}, \ldots) = -\sum_{y_t=0}^{R_{Max}} \sum_{y_{t-1}=0}^{R_{Max}} \sum_{y_{t-2}=0}^{R_{Max}} \ldots p(y_t, y_{t-1}, y_{t-2}, \ldots) log_2\, p(y_t, y_{t-1}, y_{t-2}, \ldots)$$

The estimation of this entropy was performed using Monte Carlo with importance sampling. In Monte Carlo, random samples of a vector $(y_t, y_{t-1}, y_{t-2}, \ldots)$ are drawn from a proposal distribution $q(y_t, y_{t-1}, y_{t-2}, \ldots)$ and used to estimate the expected value of $\log_2 p(y_t, y_{t-1}, y_{t-2}, \ldots)$ by an algebraic average weighted by the likelihood ratio of $p(y_t, y_{t-1}, y_{t-2}, \ldots)/q(y_t, y_{t-1}, y_{t-2}, \ldots)$. The sampling stops when entropy estimations reach an equilibrium. Information estimations are also known to suffer from positive bias [42]. Here, biased-corrected estimates and errors on information values were obtained from

Jackknifing the estimation of the time-varying rates and bootstrapping the Monte Carlo samples.

For these calculations, one has also to determine the size of the time window used for estimating the instantaneous information and correspondingly the steps for the cumulative information. This time window is used to estimate spike counts and the average rate $\mu_{s_i}(t)$ and depends both the dynamics of the stimulus and on the response properties of the neurons. By performing a coherence analysis on spike trains and a power spectral analysis on time varying rate in response to natural stimuli, we found that 10 ms (or 50 Hz) captured between 97% and 99% of the dynamics in our system (see methods and Sup. Fig. 1).

Finally, we also estimated the information values for stimulus categories by performing the weighted sum of probabilities for stimuli belonging to each category. The information about categories at time *t*:

$$I_t = H(Y_t) - H(Y_t|C).$$

is obtained from the conditional probability of response given the category c_k, which is in turn calculated as the average conditional probability of response for the stimuli belonging to that category:

$$p(y_t|c_k) = \sum_{s_k} p(s_k)p(y_t|s_k)$$

Here, $p(s_k)$ is the probability of occurrence of stimulus s_k within the category c_k. In controlled playback experiments (as here), $p(s_k)$ is $1/n_{s_k}$ where $n_{s_k}$is the number of stimuli used to sample category c_k. Similarly, $p(c_k)$, the probability of occurrence of vocalizations in category c_k was taken as $1/n_c$ where n_c is the number of categories. In our system, the stimuli are individual renditions of vocal communication calls that fall into 9 call categories of the zebra finch vocal repertoire. We will contrast stimulus information to categorical information, both instantaneous and cumulative for these behaviorally relevant categories of

304 call-types.

305 ## Time-varying information for model neurons.

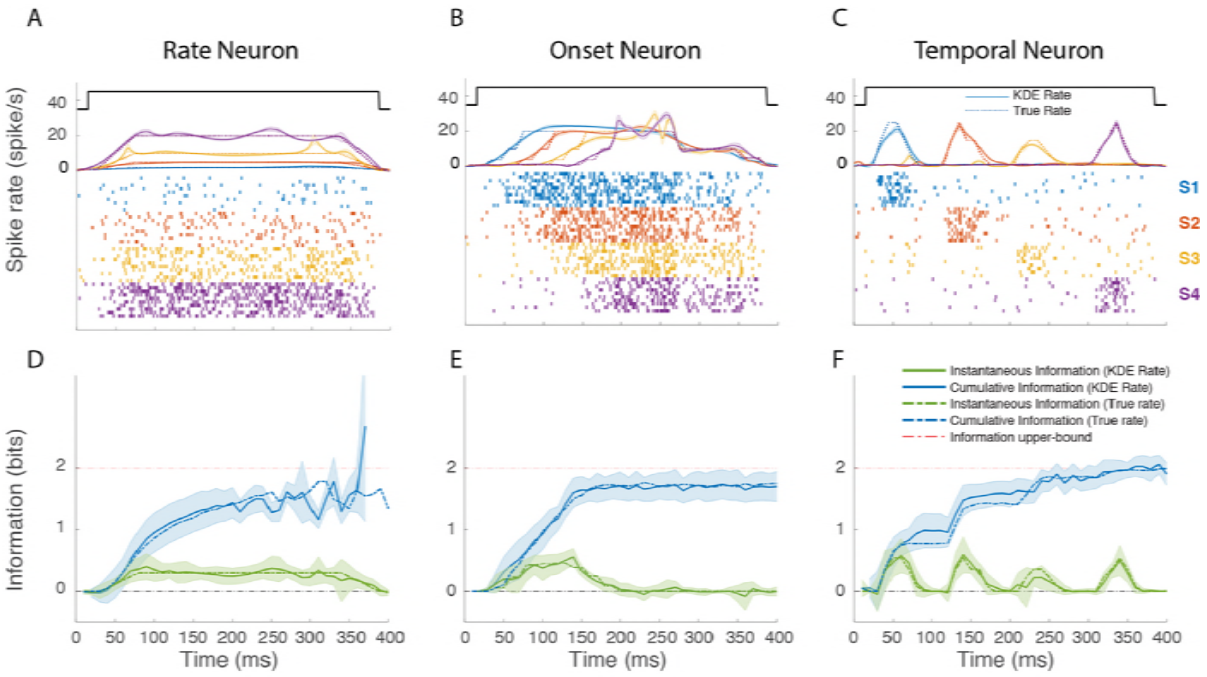

Figure 1. Instantaneous and Cumulative Information for 3 Model Poisson Neurons. The *top row* (**A,B,C**) shows the firing rate and simulated spike rasters of 3 model neurons to 4 hypothetical stimuli (S1-S4). The onset and offset of all stimuli are identical and shown by the top solid black line. The model rates for the four stimuli are shown in colored dotted lines. These rates are used to generate spike patterns using an inhomogeneous Poisson process. Ten realizations for S1-S4 are shown as spike rasters. The rate recovered from those rasters using a time-varying kernel density estimate (KDE) are shown as colored solid lines. The shaded area around each line indicate the error on the KDE rate estimated by the standard error on the Jackknife estimates. The *bottom row* (**D,E,F**) shows the instantaneous and cumulative information obtained using either the true model rate or the recovered rate from KDE. The error bars in the instantaneous information calculations were obtained by jackknifing the KDE estimates. For the cumulative information calculations, the Monte Carlo simulations were repeated for each jackknife estimate. The error bars therefore include both the errors in the estimation of the true rate from spike rasters (data limitation) and the errors in the estimation of the cumulative information due to limited sampling (computational limitation). The time-varying response rates were chosen to illustrate neural representation for stimuli using different neural codes labelled here as *Rate* (**A, D**), *Onset* (**B, E**), and *Temporal* (**C, F**).

306 To validate our approach and to illustrate the behavior of time-varying information

307 values, we calculated instantaneous and cumulative information for model neurons with

simple and stereotyped response properties. Figure 1 shows the firing rates, raster plots and information values for 3 model neurons in response to 4 stimuli (S1-S4). One model neuron responds to the 4 stimuli with different mean firing rates that are constant in time (Rate Neuron). A second model neuron responds to the four stimuli with the same fixed firing rate but with different latencies (Onset Neuron). The third model neuron also responds with equal average firing rates to the four stimuli but the response occurs at different times (Temporal Neuron).

These simulations illustrate some very basic principles of neural coding. First, many different response profiles can lead to very similar rates of information: in all three simulations, the cumulative information approaches the maximum possible value (2 bits). Second, the coding capacities of neurons are a function of both the range of firing rates that can be achieved (as in the rate neuron) and the modulations in time of this neural activity. Third, the estimation of the instantaneous information gives an incomplete picture of the neural coding of a neuron as it does not incorporate the redundancy or independence of the neural representation over time. For example, on the one hand, comparing the instantaneous information in the Rate neuron to that of the Onset neuron, one might erroneously conclude that the Rate neuron has more information while, in fact, the cumulative information shows that the Onset neuron is more informative at short time scales. On the other hand, one can also observe that the cumulative information in the Rate neuron continues to increase while the firing rate is constant; additional time points allows for a better assessment of that firing rate by time-averaging out neural noise.

These simulations also allowed us to validate our methods. The KDE for the empirical estimation of the time-varying rate based on the generated spike rasters (solid line) gave very good predictions of the actual model rates (dashed lines): over all stimuli and model neurons, the average error was less than 0.02 spikes/ms. Not surprisingly then, using

the actual rate versus the estimated rate yielded practically identical results in the information calculations (dashed vs solid lines). We also checked that the bias corrected estimates were accurate: the instantaneous information was indeed centered at zero when the response to the 4 stimuli was identical. We verified that the actual values of instantaneous and cumulative information were correct. For example, in the Temporal neuron a peak instantaneous information of 0.5 bits is expected as 1 out 4 stimuli will be almost perfectly discriminated. Finally, we also assessed the limitations of Monte Carlo with importance sampling for the estimation of the cumulative information. For neurons, with continuously high firing rates, this estimation can become unreliable at longer integration times as illustrated by the calculation for the Rate neuron. However, in those cases, the estimate of the standard error also increased drastically and allowed us to define end points for the calculation of the cumulative information.

Avian auditory neurons have Poisson statistics.

Since our estimation of the time-varying information values was based on a Poisson parametrization for the distribution of spike counts, we first assessed the validity of this assumption. Given the small number of trials, we could only assess whether the first and second moments (mean and variance) obeyed Poisson statistics. Figure 2 shows the Fano Factor estimated at consecutive time points after stimulus onset and both for individual stimuli (onset) and average across stimuli. The mean Fano factor for the population was 1.04 with SEM of 0.04.

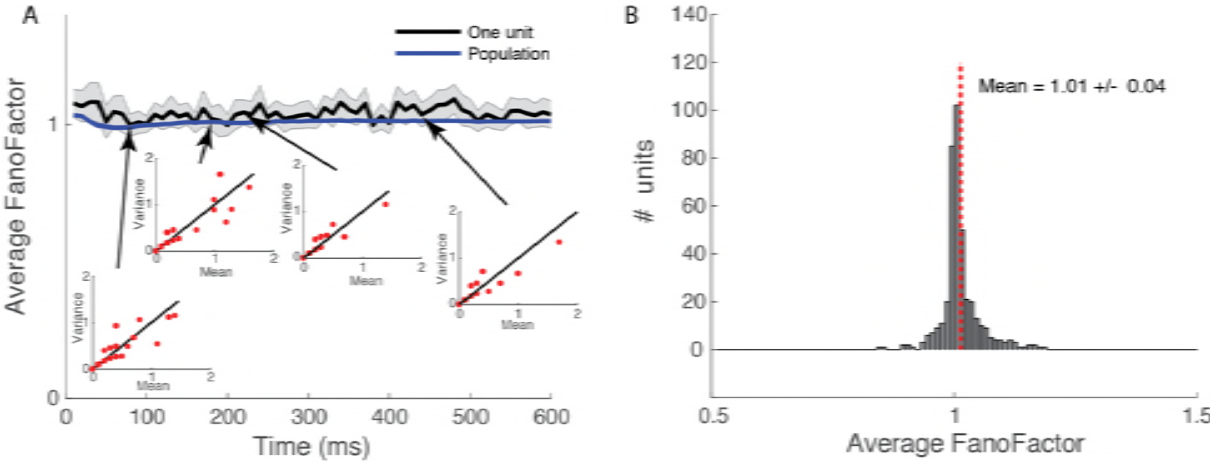

Figure 2. Avian Auditory Neurons have Poisson Statistics. **A.** Time-varying Fano Factor (Variance/Mean) obtained from the empirical distribution of spike counts estimated in successive 10 ms windows. Spike count distributions are obtained from 10 trials and the average Fano Factor from repeating the estimation of mean and variance calculation for all stimuli presented (min=54, max=104). The Fano Factor is shown for one example neuron (solid black line) and also averaged across the entire population (n=404). Error bars are ± two SEMs. The insets show the mean and variance spike count for the example neuron at a given time shown by the arrows. On those plots, each red dot corresponds to one stimulus (many points overlap). **B.** Distribution of time averaged Fano Factors for the population of neurons (n=404). Fano Factors are not significantly different from 1.

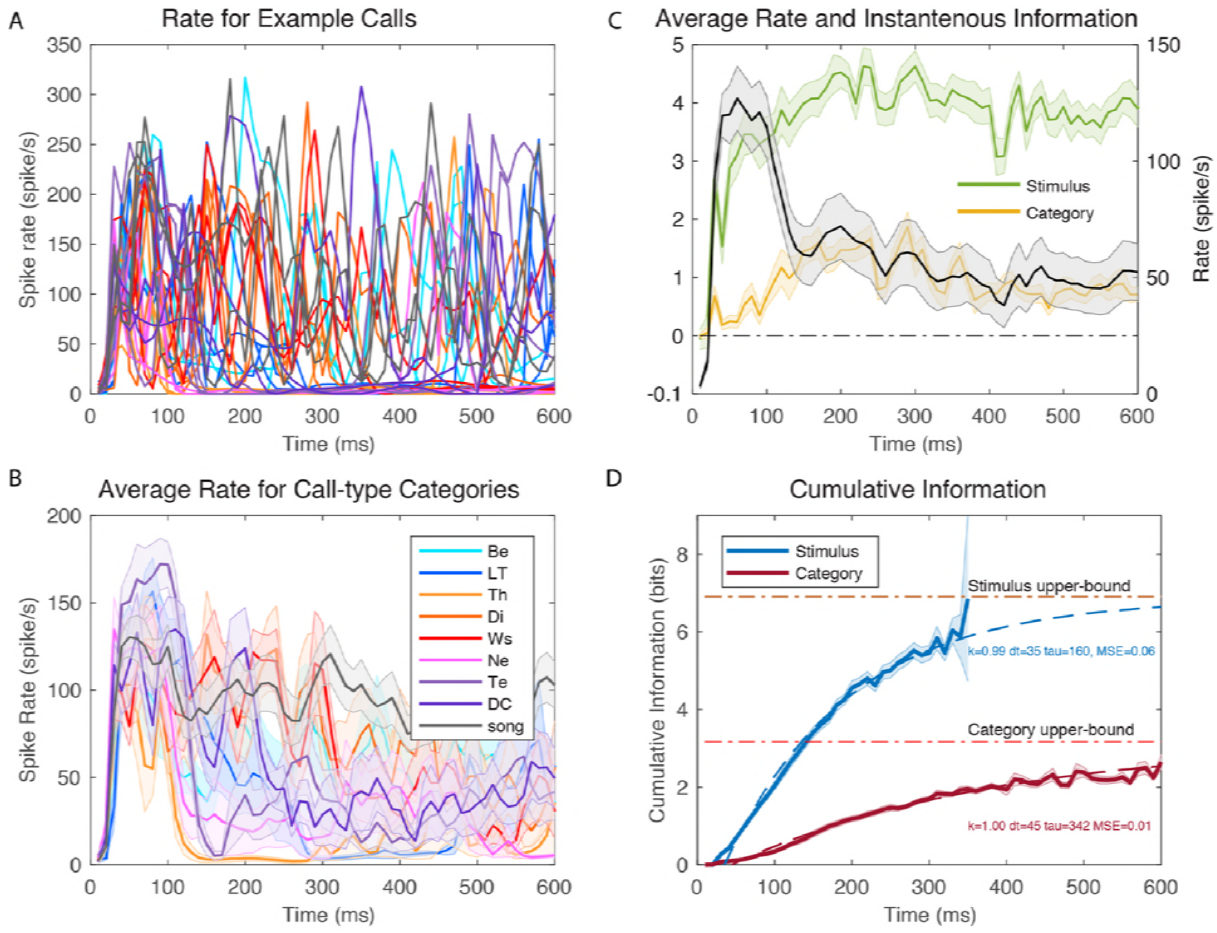

Figure 3. Time-varying Firing Rates and Information Values for Example Neuron 1. A. Time-varying firing rate obtained from kernel density estimation (KDE) of ten repetitions of different example stimuli. The plot shows the responses to two examples of calls from each call-type: 18 time series color coded by call-type using the color scheme shown in the legend of B. 0 ms corresponds to stimulus onset. **B.** Averaged time-varying firing rate obtained for each call-type category. These average responses are obtained by averaging the KDE estimates of firing rates for each stimulus belonging to the same call-type (~ 10 example stimuli per call-type). Shaded error bars show ± one SEM. **C.** The overall (averaged over all stimuli) time-varying firing rate for the same example neuron is shown by the solid black line (right y-axis) with ± SEM as shaded error bars. The green line and yellow line (left y-axis) correspond to the instantaneous information for stimuli and call-type categories calculated in successive 10 ms windows. Shaded error bars were obtained by a jackknife procedure **D.** Cumulative information for stimuli and call-type categories for the same example neuron. The shaded error bars are ± SE obtained by jackknifing and resampling (see Fig. 1 and Methods). Each cumulative information curve is also fitted using an exponential function (dashed lines) characterized by three parameters: a latency (dt, in ms), an exponential rate (tau, in ms) and the infinite time limit value expressed as a fraction of the maximum information achievable (k). The MSE is the mean square error of the fit in bits. This example neuron had a very high stimulus evoked mean firing rate with rapid and reliable time-varying dynamics leading to high information rates. Spontaneous firing was very low (~0 spikes/s). Spike rasters for this neuron are shown on Sup. Fig. 4.

354 Time-varying Information for 3 example neurons.

355 In Figures 3-5, we show the time-varying firing rates, the time-varying instantaneous

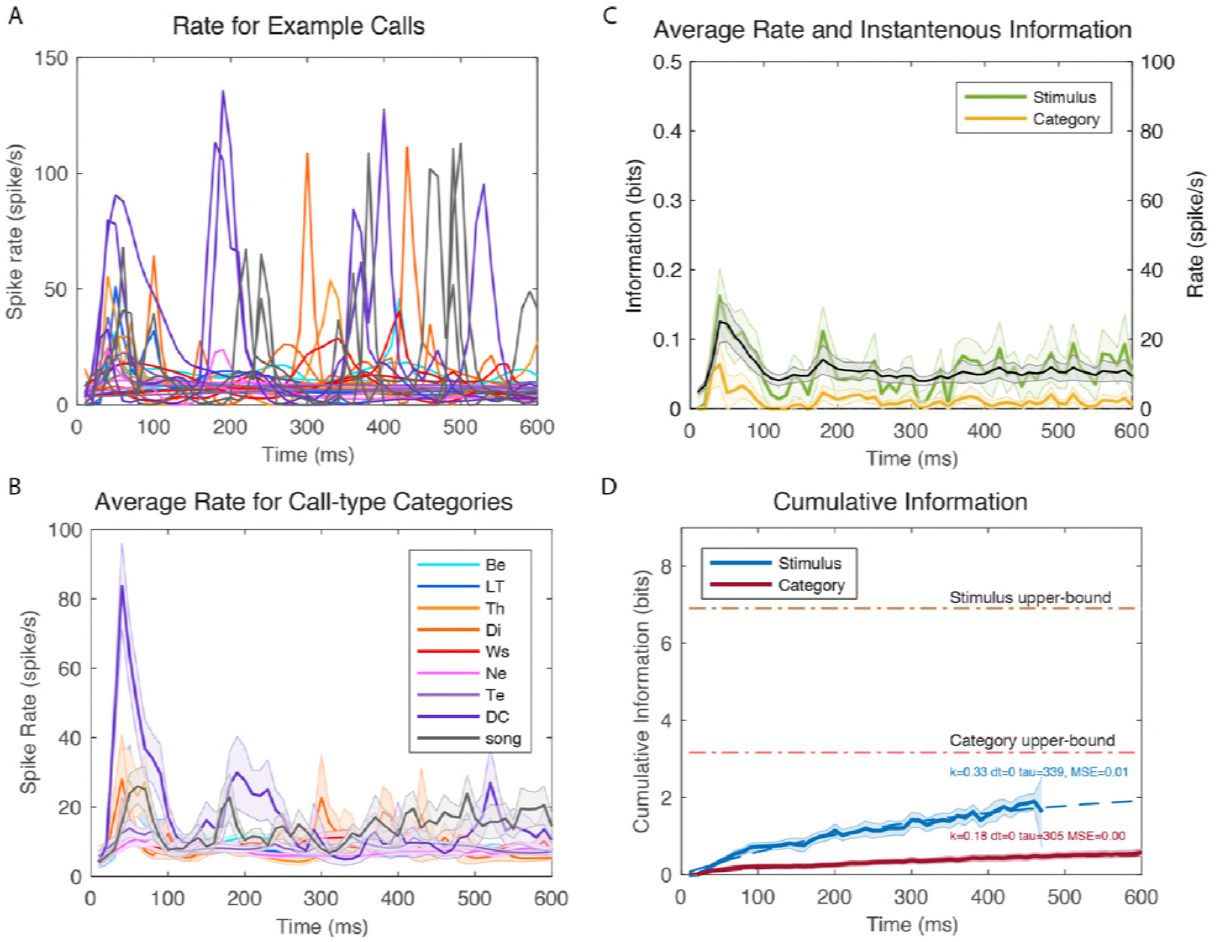

Figure 4. Time-varying Firing Rates and Information Values for Example Neuron 2. As in figure 3 but for a neuron with lower firing rates and displaying selectivity for Distance Calls. Spike rasters for this neuron are shown on Sup. Fig. 5.

356 information and the cumulative information for 3 zebra finch auditory neurons with distinct

357 response properties. The neuron in Figure 3 responded robustly to all communication calls

358 with high and reliable firing rates. It also responded in a time locked fashion sometimes at

multiple time points for single calls. Although this neuron was not selective for a particular stimulus or call-type category, by combining rate and temporal codes it reached very high levels of instantaneous information. Moreover, this instantaneous information showed little redundancy yielding very high cumulative information. One can also observe, that for this particular neuron, the average time-varying firing rate is not correlated with instantaneous

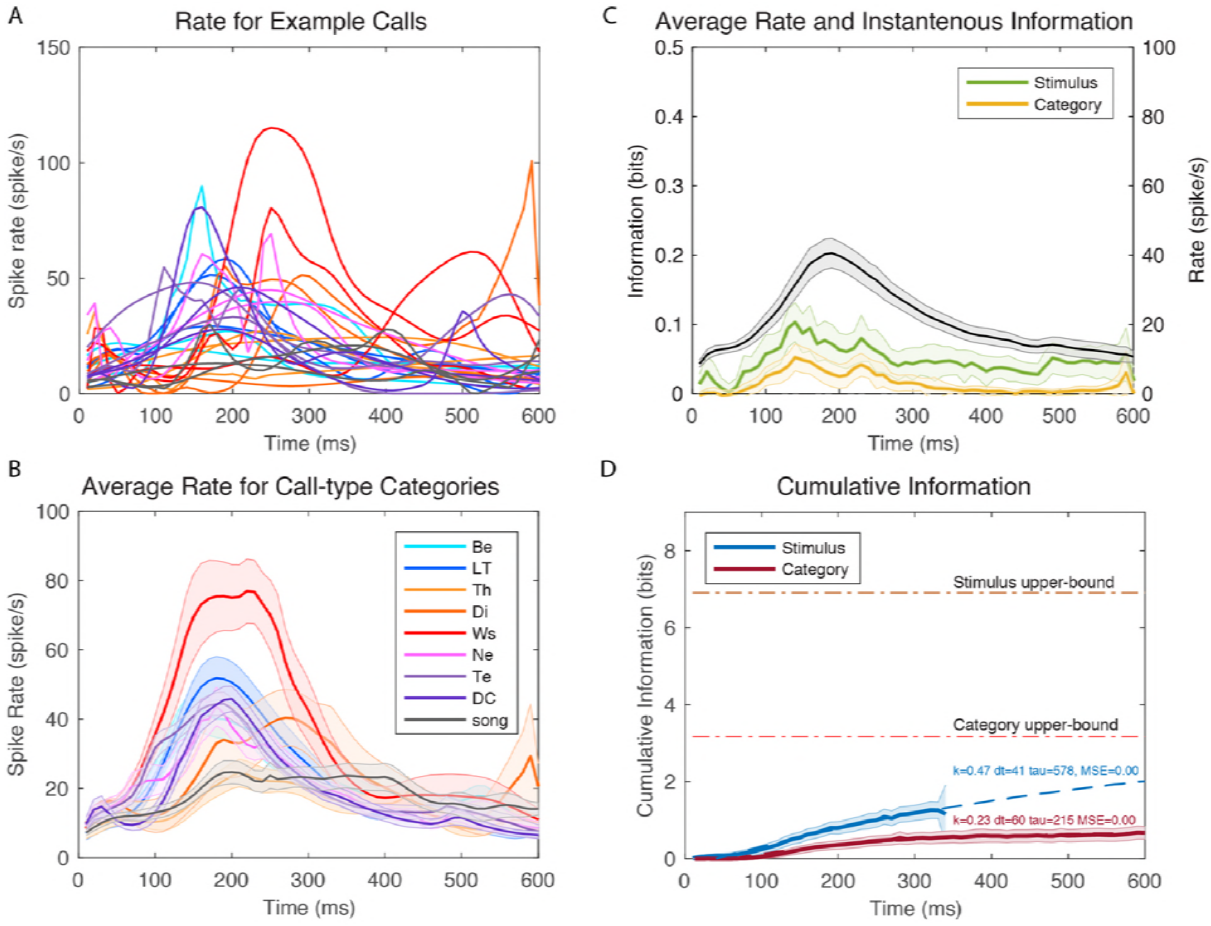

Figure 5. Time-varying Firing Rates and Information Values for Example Neuron 3. As in figure 3 but for a neuron with intermediate firing rates and displaying selectivity for Wsst (Ws) or Aggressive Calls. Note also the longer latency relative to the neuron shown in 3 and 4. Spike rasters for this neuron are shown on Sup. Fig. 6.

information. This neuron shows a strong onset response in its firing rate while the instantaneous information is almost constant and even slightly lower during the onset response. The neurons in Figures 4 and 5 have much lower firing rates and exhibit selectivity for a call-type, the Distance Call (DC) and the Wsst Call (Ws) respectively. The neuron in

Figure 4 exhibits both an onset and sustained response both of which are selective for DC. The neuron in Figure 5 has a much longer latency for response with correlated peaks in firing rate and instantaneous information found between 100 and 300 ms after stimulus onset (Example of spike rasters from single trials for these three neurons are shown in Sup. Figs. 4-6).

The cumulative information curves were fitted with an exponential function that allows us to quantify the time constant of information accumulation (τ), the saturation level (k) relative to the maximum information that could be achieved (I_{Max}) and the latency (dt):

$$CI_{mod}(t) = kI_{Max}(1 - e^{-(t-dt)/\tau})$$

Most of the calls in the zebra finch repertoire have durations that are shorter than 300 ms [39]. In order to investigate the cumulative information accumulated at this behaviorally relevant fixed point in time, we estimated the relative cumulative information as the value of the model at 300 ms relative to I_{Max}.;

$$k(300) = CI_{mod}(300)/I_{Max}.$$

The results of the fit are shown in dashed lines in the cumulative information plot for each neuron. One can observe that the neuron in Figure 3 has exceptionally high values of saturation: with sufficiently long integrations time, single spike trials could be used to perfectly assess what stimulus (out of those used in the experiment) was hear and, thus, which call-type category it belonged to. The selective neurons in Figures 4 and 5 have much lower saturation levels as expected since they mostly respond to stimuli from a single call-type category. The neuron in Figure 5 has longer latency in its categorical cumulative information but this is not the case for the neuron in Figure 4 that has a rapid yet selective onset response. The high firing neuron (Figure 3) also has a faster time constant τ for the stimulus information than the selective neurons shown in Figures 4-5. All three neurons have

392 similar and relatively slow time constants for the categorical information in the 200-300 ms
393 range.
394
395 ## Rate and Time-Varying Information: Population Analysis

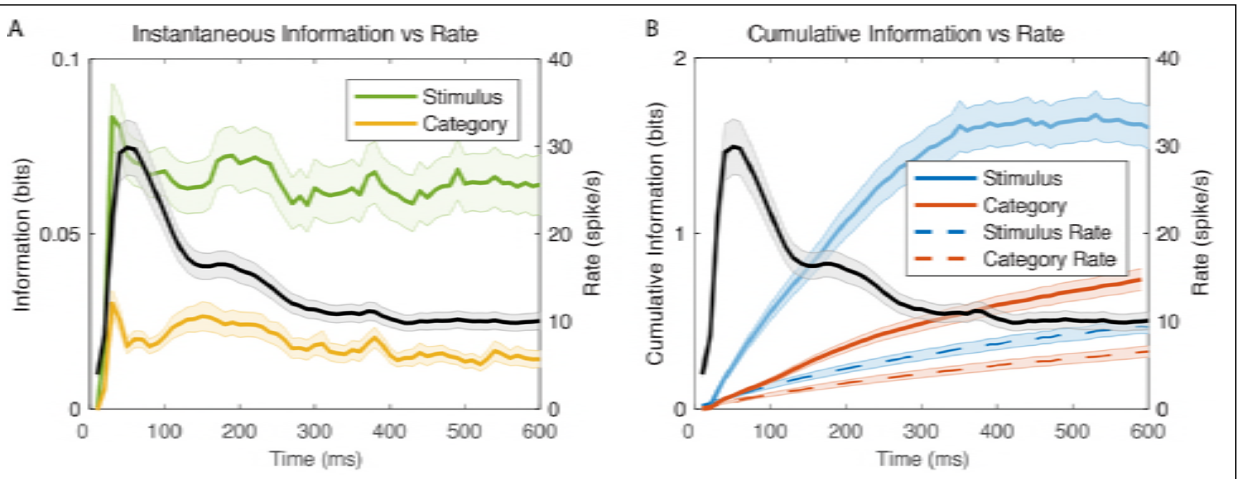

Figure 6. Time-varying Firing Rates and Information Values for the Population. A. The solid black line (right y-axis) shows the time-varying firing rate averaged across all neurons (n=337) and all stimuli played. The shaded error bars are ± SEM. The green and yellow lines (left y-axis) show the instantaneous information for stimuli and call-type categories respectively. The shaded error bars are ± SEM. **B.** The time-varying mean firing rate is shown as in A. The blue and red solid lines show the population average cumulative information for stimuli and call-type categories respectively. The blue and red dashed lines show the corresponding average cumulative information values calculated with constant averaged firing rates for each stimulus for each neuron over the first 600ms after stimulus onset (a rate code). The shaded error bars are ± SEM.

396 Figure 6A shows the time course of the firing rate averaged across all stimuli and its
397 relationship with the instantaneous information. On average, avian cortical auditory neurons
398 show an onset response followed by a sustained response as observed at many stages of
399 auditory processing and in many sensory systems. The instantaneous information, however,
400 remains almost constant during the entire time. This is true both for the information about
401 individual stimuli or the information about categories. Thus, the onset response is only less
402 selective/informative than the sustained response in bits/spike but not in bits/s; when
403 processing natural vocalizations, the onset and sustained response are equally informative.

Moreover, the information in the sustained response continues to provide new information as reflected by the continuous and relatively fast increase in cumulative information shown in Figure 6B. That rapid rate of increase should be compared to the one observed when the mean firing rate for each stimulus estimated across the entire time-window was used in the calculation (dashed lines in Fig. 6B). As seen in those curves, the increases in the cumulative information for the rate code is much smaller (the information still increases because of noise averaging as explained above). The time-varying rates observed in neural responses (as illustrated in Fig. 3A) provide additional information. How much more? For the coding of individual stimuli (comparing the dashed blue line to the solid blue line in Fig. 6B), a fixed rate code (or assumption) captures only 24% of the information at 100 ms and 21% at 300 ms. The effect for categorical information is smaller because some of the coding dynamics in time-varying responses to stimuli belonging to the same category effectively become neural noise: for categorical information, a fixed rate code captures 50% of the information at 100 ms and 41 % at 300 ms.

The distributions of time constants, τ for the cumulative information for stimuli and call-type categories are shown on Figure 9. The distributions of relative cumulative information at 300ms (k(300)) are shown on Figure 10.. The range of time constants observed across the population of neurons was large (100 ms-600 ms) with average time constants of 459 ms for cumulative stimulus information and 372 ms for cumulative categorical information. This difference in means of time constants is statistically significant (Paired t-test $t(214)=3.49$, $p=0.00058$); the ongoing time-varying rate changes continue to provide more information for decoding stimuli and less so for decoding categories of stimuli. There is also a wide distribution of relative cumulative information values (k(300) ranging from close to zero to 0.6 . On average across neurons, the k(300) was 0.2 (or 20%) for stimuli and 0.15 (or 15%) for categories. These differences in relative information values are highly

significant suggesting that, single neurons, capture more variability in stimuli than in categories. Note however that measures of relative information depend on the number of stimuli or categories. Therefore, a direct statistical comparison is not warranted. The comparison between stimulus representation and category representation requires estimations of expected values of categorical information given stimulus information which is performed below. Relative cumulative information values can, however, be used for stimulus and categories independently to assess other coding properties: although average time-varying rates and instantaneous time varying information are not well correlated within single neurons (as shown in Figs. 3 and 6), the relative cumulative information is correlated with average firing rates. For cumulative stimulus information, one finds an increase in k(300) of 1% per spike/s (Adj R^2=0.36, F(1,213)=120, p=1.82 10^{-22}) and, for cumulative categorical information, an increase in k_{300} of 0.8% per spike/s (Adj R^2=0.34, F(1,213) = 112, p = 2.26 10^{-21}).

454

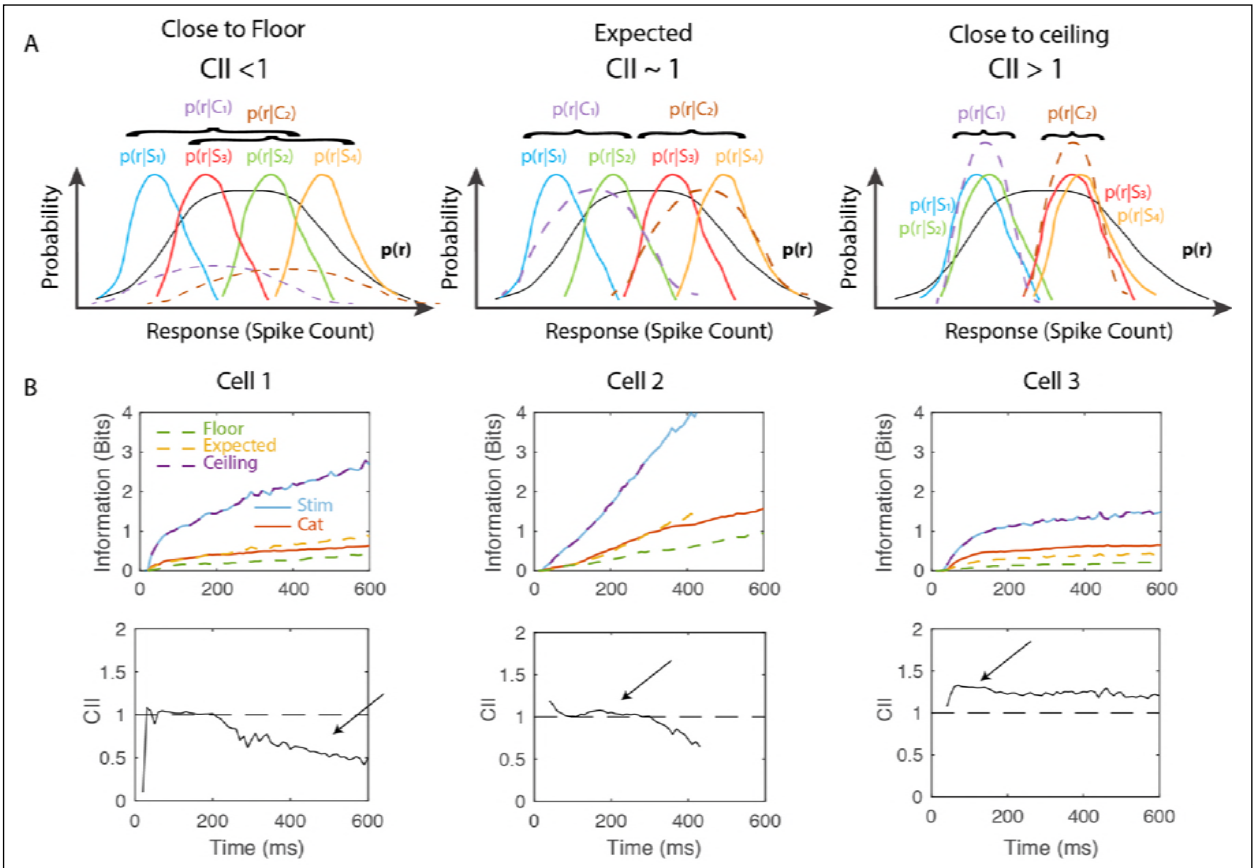

Figure 7. Cumulative Information and the Categorical Information Index. A. Schematic of hypothetical response probability distributions that yield different values of the Categorical Information Index (CII). CII is defined by comparing the cumulative categorical information to a floor (CII = 0), an expected value predicted from the stimulus information (CII=1) and a ceiling value (CII = 2) as described in the text and methods. Each plot represents the distributions of hypothetical neural responses for different stimuli (S1 to S4) that yield different values of CII. When stimuli are grouped randomly into categories (S_1 and S_2 belong to C_1, while S_3 and S_4 belong to C_2), CII is close to 0 (left panel). When stimulus categories preserve the order of the stimulus conditioned response distributions and these distributions are equally separated, effectively coding for both stimuli and categories, CII is equal to 1 (middle panel). When stimuli belonging to the same category have identical responses, the stimulus information is equal to the category information, the response being effectively invariant within categories and CII is equal to 2 (right panel). Note that the actual response probability distributions are multidimensional (one dimension for each time lag) with Poisson marginals. **B.** Example of the cumulative information for stimuli and call-type categories and CII for 3 different representative neurons. The blue and red lines are the cumulative information for stimuli and categories respectively. Estimates of the floor (dashed-green), expected (dashed-orange) and ceiling (dashed-purple, here overlapping with blue) values for the categorical cumulative information as described in A are given as well. The CII is shown as a solid line in the second row for each example neuron. Cell 1 has long periods of time with CII < 1, Cell 2 has long periods of time with CII ~ 1 and Cell has long periods of time with CII > 1 as shown by the arrows.

Analysis of the Categorical Information

We are interested in identifying neurons that could play an important role in categorizing vocalizations. We had previously identified example neurons that were highly selective for particular call-types and showed a high degree of invariance such as those shown in Figures 4 and 5 [40]. Here, we attempted to quantify the neural invariance for call renditions within call-type categories along time. For this purpose, we computed a Categorical Information Index (CII). The CII compares the actual categorical cumulative information to three potential values: a floor or minimum value (set at 0), an expected value for shared information between stimuli and categories (set at 1) and a ceiling or maximum value (set at 2). The floor is the categorical information that one would obtain if stimuli are randomly grouped. The shared-information value is the information that one would obtain if the information about stimuli is equally shared across all stimuli and the neural responses for stimuli are perfectly sorted for each natural call-type category; for example, at a given point in time the 10 renditions of DC would elicit the 10 highest rates, the 10 renditions of LT call the next 10 higher firing rates and so forth. This shared-information value does therefore assume that, for a given neuronal signal to noise ratio, neural responses segregate categories maximally while also preserving the maximum discrimination between stimuli within categories. The ceiling value is the categorical information value that one would obtain if a maximum amount of information about stimuli was used for the discrimination of categories and a minimum for discriminating stimuli within categories; it assumes maximum invariance to variations within a category. The ceiling value is equal to the stimulus information until it reaches $\log_2(n_c)$, where n_c is the number of categories, corresponding here to the 9 call-types.

Figure 7B shows the time-varying floor (dashed-green), shared (dashed-orange) and ceiling (dashed-red) values of cumulative categorical information along with the actual stimulus (solid blue) and categorical (solid red) cumulative information for 3 neurons chosen to illustrate CIIs that are below 1, around 1 and above 1. Figure 7A shows cartoon probability distributions of neural responses for particular stimuli and particular categories that correspond to the floor, shared and ceiling values.

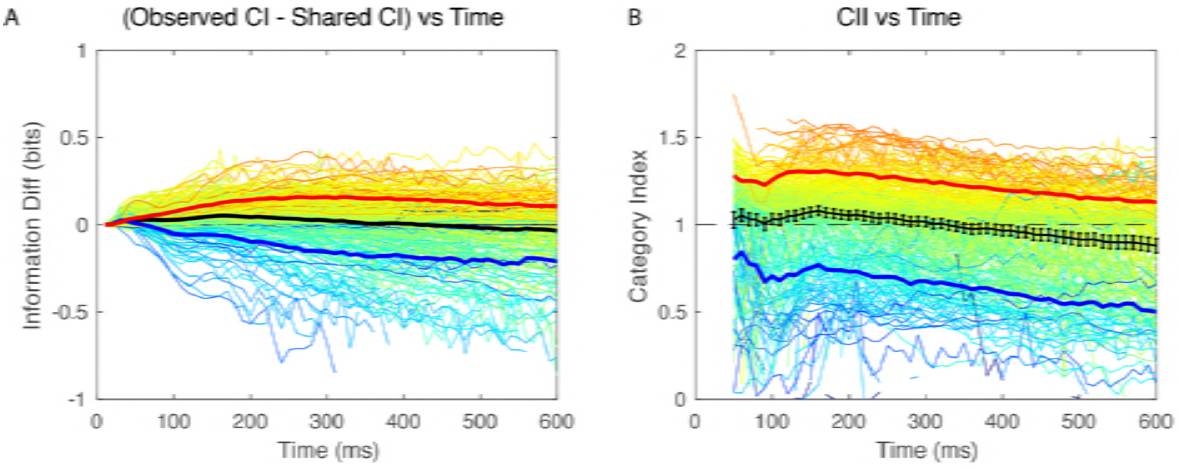

Figure 8. Categorical Cumulative Information. As explained in Fig. 7 and in the text, the cumulative information (CI) for call-type categories can be analyzed in terms of a floor or minimum value, a shared value and a ceiling or maximum value. **A.** Difference in the observed cumulative information in bits relative to the shared value. The bold black line is the average across all neurons (n=337). The thin colored lines correspond to individual neurons. Each line color corresponds to the time average Categorical Information Index (CII) of the neuron obtained between 50 and 300ms. The solid red line is the average obtained for the quartile of neurons with the highest CII and the blue solid line is average obtained for the quartile of neurons with the lowest CII. The same color code is used in B and in Figs. 9 and 10. **B.** Value of the Categorical Information Index as a function of time for all neurons in the population. Error bars on the average CII (solid bold black line) are 2 sem.

The plots in Figure 8 show the results of this analysis for the population both in absolute information units (left panel) and in the normalized units of CII. The thin colored lines correspond to CII curves for single neurons and they are colored according to the time average CII. The average CII over neurons (bold line on right panel) is very close to the shared value of 1 as one might expect if acoustical differences across stimuli drive neural

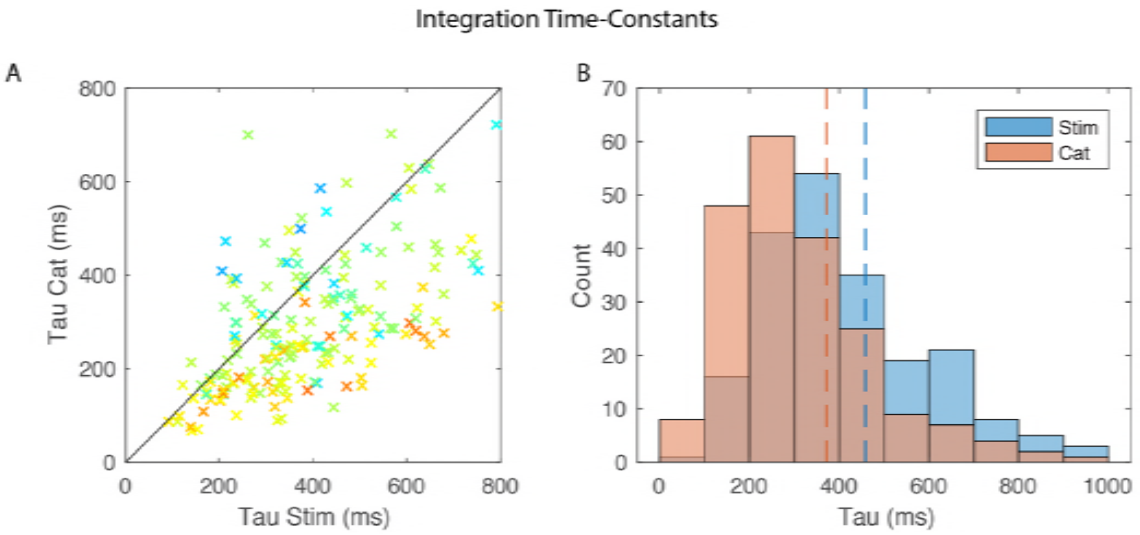

Figure 9. Time constants for Cumulative Information. For a large fraction of neurons (214/337 neurons), cumulative information for stimuli and call-type categories were well fitted with exponential curves. **A.** Scatter plot of the time constant of the exponential fit for stimuli (Stim – x axis) versus call categories (Sem – y axis). Single data points are colored according to the time averaged CII of each neuron (see Fig 8). **B.** Histogram of the two distributions of time constants. Dashed lines indicate the mean of each distribution (Stim = 459 ms; Cat = 372 ms).

responses in a linear fashion along some acoustical feature *and* call categories segregate perfectly along that same acoustical feature. The average CII is slightly (and significantly) above 1 between 120 and 260 ms showing some small degree of average invariance for call renditions within a call-type category during those times. Focusing, on the 25% of neurons with the highest CII, we found a peak at 175 ms. More significantly, perhaps, it is clear that there is a wide distribution of CII around the shared value of 1. However, this distribution includes many neurons that exhibit a high degree of invariance for call renditions within call-type categories as shown by the average CII for the top quartile (red solid line). For that top 25%, the absolute value of additional categorial cumulative information relative to the expected shared information value reaches a maximum of 0.16 bits at 320 ms (Figure 8A).

Do these high CII neurons exhibit other characteristic response properties? In the scatter plots of Figures 9 and 10, we examined the relationship between CII (color coded) and, respectively, time constants and relative level of the cumulative information. It can be

seen from Figure 9, that neurons with high CII have relatively long stimulus time constants in comparison to their corresponding time constant observed for categorical information. This relationship is also significant for the entire population of neurons (Linear Regression explaining CII from τ_{cat}/τ_{stim}: Adj R^2=0.11, F(1,213) = 28.5, p=2.37 10^{-7}). As shown in Figure 10, neurons with high CII also have higher relative levels of categorical information in comparison to their relative values for stimulus information although this result is expected given our definition of CII (Linear Regression explaining CII from $k_{cat}(300)$-$k_{stim}(300)$: Adj R^2=0.76, F(1,213) = 675, p=5.5 10^{-68}). Finally, one can also notice that neurons with high CII have low values of relative cumulative information (Linear Regression explaining CII from $k_{stim}(300)$: Coef = -0.84 Adj R^2=0.28, F(1,213) = 84, p=3.96 10^{-17}). This effect is caused by the correlation between invariance and selectivity as we have shown previously[40]: neurons that show the highest degrees of invariance also tend to respond to a small number of call-type categories and thus a small number of stimuli. As such, high invariance and high selectivity goes hand in hand with lower values of information.

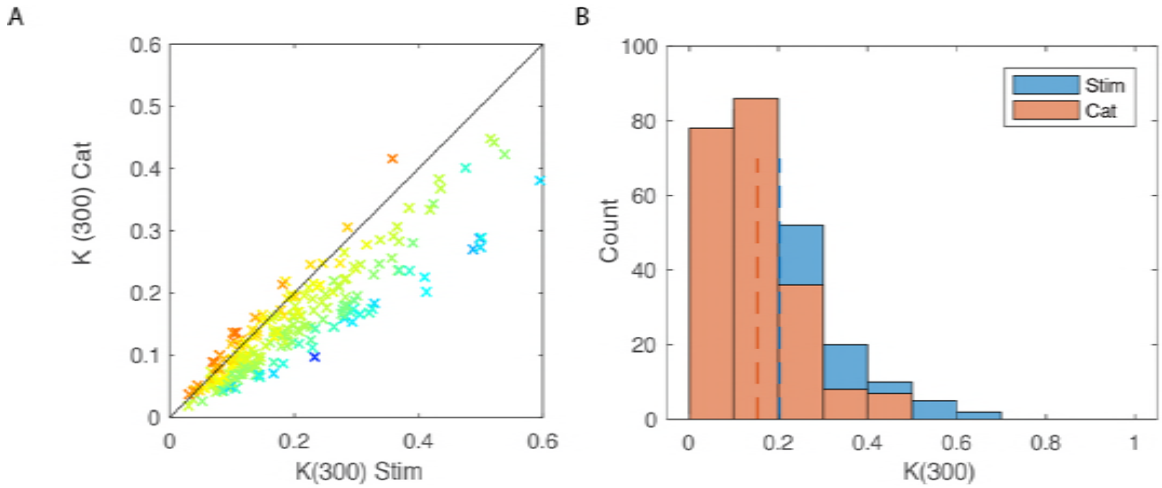

Figure 10. Distribution of Relative Cumulative Information estimated at 300 ms. For a large fraction of neurons (214/337 neurons), cumulative information for stimuli and call-type categories were well fitted with exponential curves. Here we used these fits, to estimate the cumulative information obtained at 300 ms relative to the maximum achievable information ($\log_2(n_{stim})$ or $\log_2(n_{cat})$), k(300). k(300) is a number between 0 and 1 **A.** Scatter plot of k(300) for stimuli (Stim – x axis) versus categories (Cat – y axis). Single data points are colored according to the time average Categorical Information Index (see Figs 7-8). **B.** Histogram of the two distributions of k(300). Dashed lines indicate the mean of each distribution (Stim = 0.2; Cat = 0.15).

Anatomical Organization

We examined whether neurons were organized in the avian auditory cortex based on their CII, cumulative information time constants (τ) and saturation levels (k). Most of our recording sites were identified histologically and could be assigned to avian cortical areas that had been segregated into the thalamic recipient area, L2; intermediate primary auditory regions, L1, L3, CML and L; and secondary areas, CMM and NCM [43-46]. We also obtained spatial x,y,z coordinates of the recording sites relative to the midline, the position along the rostral-caudal axis where the lamina pallio-subpallialis LPS) is the most dorsal, and the top of the brain (Fig. 11).

In all regions, we found a range of CII and thus only weak anatomical trends across areas. Using the L2 dorsal-ventral oblique axis as reference point, CII was slightly higher as one moved rostrally or caudally to higher regions of auditory processing (Linear Regression: Adj R^2= 0.03, F(3,194)=4.19, p=0.016). However, an ANOVA also suggested that both regions NCM and L2 had slightly higher mean CII (Adj R^2=0.027, F(4,185) = 2.77, p=0.042). We also observed an increase in the time constant (τ) for the stimulus cumulative information that parallel the increase in CII as one moved away from the L2 axis (Linear Regression: Ajd R^2=0.03, F(3,194)=4.79, p=0.0093). These significant anatomical trends were characterized by very small effect sizes. We also did not find any anatomical organization of saturation constants (k) for the cumulative information; neurons that had high levels of information could be found next to neurons with much lower levels and similar levels of average information were found in all regions.

539

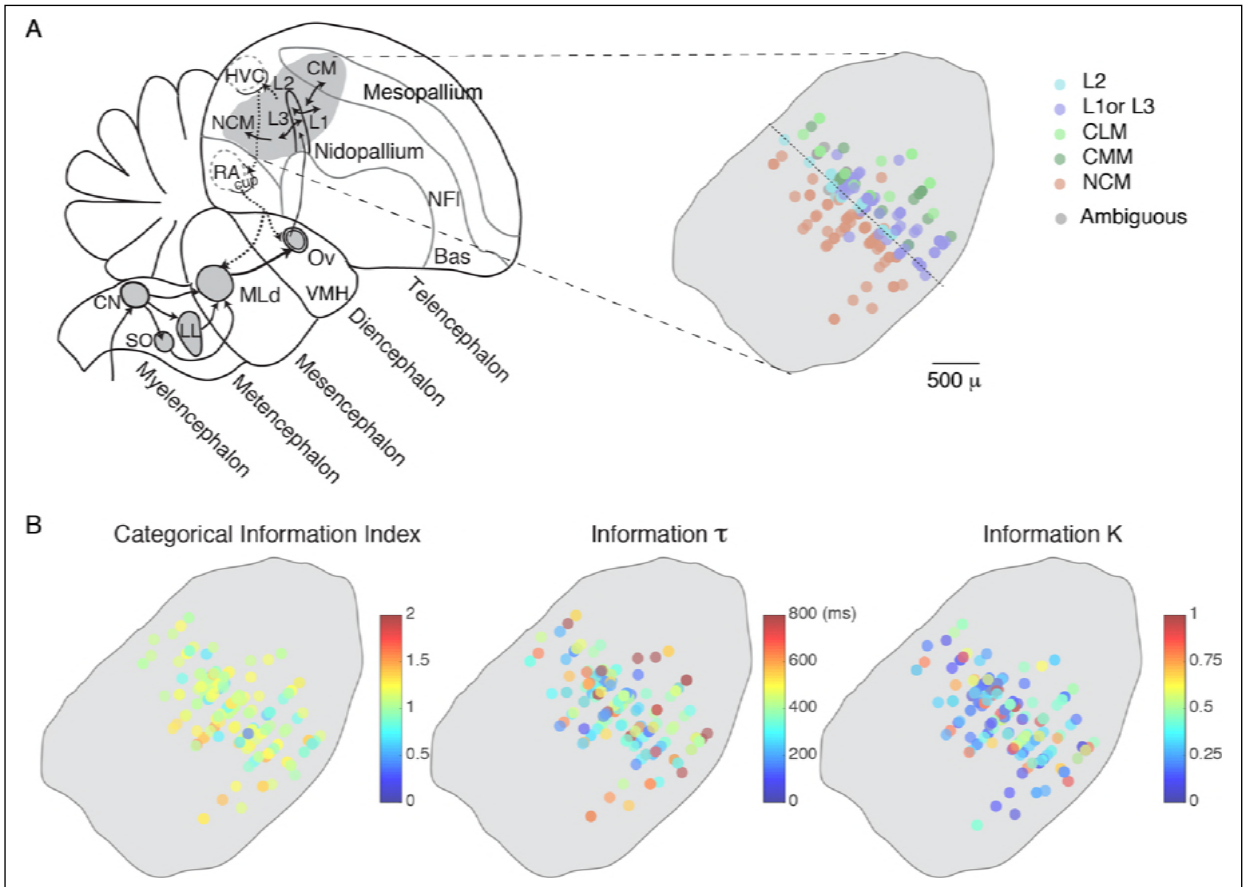

Figure 11. Anatomical Organization. A. The left panel is a schematic of the different processing stages in the ascending avian auditory system (grey areas) shown on a parasagittal view. Our recording sites were from the primary and secondary avian auditory cortical areas (the auditory pallium) and are shown on the right panel. The recording sites from different birds were aligned in the rostral-caudal dimension using the oblique rostro-caudal *long* axis of L2 (dotted line). Recording site positions also varied along the medial-lateral dimension (in and out of the page) and are all superimposed here. **B.** Functional anatomical maps of the Categorical Information Index, the time constant τ and saturation value κ of the cumulative information for stimuli. Each site is colored according to the value(s) of the variable being displayed. Transparency is used to reveal overlapping sites in this view as well as, potentially, combination of single units that were recorded from the same electrode and site.

540

541

Discussion

We modeled responses that are observed in the auditory system as inhomogeneous Poisson processes in order to estimate the time-varying instantaneous and cumulative information for vocalizations used in communications. We showed that using Kernel Density Estimation for the time-varying firing rate and Monte Carlo with importance sampling for estimating probabilities, we were able to obtain accurate and bias-free estimates of these time-varying information values. This parametric approach is powerful because a relative small number of trials can be used to estimate the time-varying response and thus information values can be estimated in response to a relative large set of stimuli (here over 100 distinct vocalizations) given typical recording times. Poisson statistics were observed in the auditory cortical neurons recorded here when they were stimulated with short natural communication calls. More generally, the same procedures can also be used with spike trains statistics that can be parametrized with probability functions that depend only on a time varying rate such as inhomogeneous gamma or inhomogeneous inverse Gaussian [12, 47] and could also be extended to ensemble of neurons. Although Poisson statistics are often observed in neural data and will correctly fit any data set obtained from pooling responses across a large number of trials [48], it makes the strong assumption that the firing rate for a particular trial for a particular neuron depends only on time. Refractory period in spiking neurons and other correlations in single neurons or in an ensemble of neurons that are not phased locked to the stimulus (i.e. noise correlations) are common violations of this assumption. Taking noise correlations into account can increase stimulus decoding accuracies [23]. In cases where noise correlations are informative, the method proposed here would only yield lower bound estimates of information theoretic values. Alternatively, one should try the use of spike metrics measures [49] in combination with stimulus decoding approaches to then obtain measures of information from the confusion matrix of predicted versus actual stimuli [13, 40,

567 50, 51]. If spike metrics can be estimated accurately (with limited data), repeating the
568 stimulus decoding procedure for progressively longer time windows would yield cumulative
569 information values such as those calculated here but which could consider noise correlations.
570 Beyond our methodological contribution, the principal goal of this analysis was to
571 characterize the neural code in higher auditory areas for communication calls. We found that,
572 on average, auditory cortical neurons responded to these natural stimuli with time-varying
573 firing rates that exhibited an onset and a sustained component of the response. Although in
574 some situations the auditory cortex appears to respond only transiently [26, 52], our data
575 supports findings from mammalian species that have showed strong sustained responses
576 when neurons are driven by preferred stimuli [21]. Similarly, in the human superior temporal
577 gyrus, the sustained responses to speech have been shown to be more informative for
578 decoding speech phonemes [53]. Natural sounds in general have also been shown to be
579 particularly efficient at driving auditory areas [12, 54-59] and thus the presence of
580 informative sustained responses is not surprising. Indeed, in some of our most selective
581 neurons, such as the neuron in Figure 5, the onset response is missing and only the sustained
582 response is observed. More generally, and on average, we found that both the transient and
583 sustained response had information about the stimulus identity *and* that the information in
584 these two response phases was not redundant: the stimulus space of natural vocalizations is
585 very large and although the initial response provides some clue as to the nature of the
586 vocalization, new and additional information is observed in the sustained response. On the
587 one hand, one might argue that, in natural vocalizations, the sound itself is changing with
588 time. These stimulus changes occur both within calls that are made of composite notes or in
589 call bouts and song motifs made of multiple syllables. Sustained responses in such cases
590 could be interpreted as multiple onset responses (but with decreasing amplitude). On the
591 other hand, from a behavioral perspective, these communication calls correspond to a single

592 auditory object: a message from a particular individual about a particular state. From either
593 perspective, these observations and analyses illustrate the importance of using behaviorally
594 relevant stimuli when analyzing the nature of the neural code.

595 The information about stimulus identity was shown to be approximately equal in
596 bits/s in the onset and sustained response. Given that the average onset response (in spikes/s)
597 is greater that the sustained response, one might conclude that the onset coding (in bit/spikes)
598 is not as efficient. Although, this is true from the point of view of a single neuron, it is almost
599 certainly not true when ensemble of neurons is considered; the relative timing of the first
600 spike has been shown both in audition [26] and in other sensory modalities [25, 27] to be
601 highly informative. Moreover, in addition to stimulus identity other stimulus features are also
602 encoded in neural responses; the timing of the stimulus is clearly marked by the onset
603 response or transient response [22, 53, 60, 61] but other stimulus attributes such as the
604 location, fundamental and loudness/distance of the sound source are also processed in
605 auditory cortex [62-64]. It is therefore very likely that the onset response contains
606 information about stimulus features other than stimulus identity or category and, potentially
607 to a greater extent than in the sustained response (e.g. relative timing of onset). We note,
608 however, that the opposite was found for the neural discrimination of two vowel sounds in
609 the ferret auditory cortex where the onset response or early response was the most
610 informative for decoding vowel identity relative to other attributes [64].

611 Our IT analysis also revealed the importance of stimulus locked spike patterns even in
612 relatively short neural responses: in just 100 ms, the mean rate captured only a quarter of the
613 information present when time-varying firing rates are considered. Thus, our analyses
614 provide additional evidence that spiking patterns carry a significant amount of stimulus
615 information and should therefore not be ignored in the analysis of neural responses [65]. The
616 spiking precision analyzed here was relatively coarse (10 ms windows) and matched to the

time scales of the relevant dynamics in the stimulus: although zebra finch calls are much longer than 10 ms, they are complex sounds with fast spectro-temporal features [39]. Therefore, although the neural code observed here uses fast varying spike rates, it cannot be labelled as a temporal code. In a rigorous definition of a temporal code, temporal information in spike patterns must code stimulus attributes other than the stimulus dynamics [66].

The cumulative information for stimulus identity or for categories increased for sustained periods of time before saturating. These saturating curves were well fitted with exponentials and yielded relatively long-time constants of approximately 460 ms for stimuli identity and 370 ms for call categories. These *information* time constants are long in comparison to the integration times that are usually found for auditory cortical neurons; the spectro-temporal receptive fields of avian auditory neurons rarely extend beyond 50 ms [67-70] although adaptive responses on longer time scales have also been described [71-73]. Information time constants depend on the integration and adaptation time constants of neurons but *also* on the stimulus dynamics: although stimulus identity and stimulus category are fixed in time, the sound itself has time varying features that can provide additional information as time goes on. It is the triple combination of the dynamics of the natural stimulus statistics, the neuronal integration time and the neuronal signal to noise levels that are going to affect the information time constant. Natural sounds and in particular communication calls are informative objects not only because of their spectral structure but also their rich dynamical structure. The importance of time in the neural code used in the auditory system has been emphasized multiple times [74-78] and our cumulative information analysis further stresses the importance of using natural sounds or synthetic sounds that carefully match natural dynamics when probing auditory neural encoding. Ultimately, it is an information time constant that includes stimulus dynamics that should be compared to behavioral responses [18]. A behavioral assay of reaction time for all the calls in the zebra

finch repertoire has not been performed but the values of a few hundred of ms correspond to the shortest time intervals between call and call back in anti-phonal calling in paired zebra finches [79]. Although, faster times could be obtained in reaction to any sounds (e.g. startle or orientation), the processing of stimulus identity to extract the information on who is calling and what is being said might require these longer processing times.

Finally, we quantified the fraction of the information about stimulus identity that could be used for extracting the call-type category. We used that analysis to characterize neurons not only in terms of their absolute coding capacities for call-type categories but also in terms of their invariance in their response to different stimuli belonging to the same call-type category. We found that, on average, information for categories is very close to what one would expect if neural representation for stimulus identity is also segregated along call-type categories. However, we also found neurons that had a high degree of invariance and could therefore be classified as categorical. On the one hand, these categorical and invariant neurons had even longer time constants for cumulative stimulus information suggesting that they could be higher in the auditory processing stream. On the other hand, we did not find a separate population of invariant neurons across all of our recordings of neurons informative for categories: the distribution of our categorical index was unimodal. Moreover, we found only weak anatomical correlations with very small increases in the Categorical Information Index along an anatomical axis corresponding to lower vs higher auditory areas. Higher avian auditory cortical areas have been associated with more complex spectro-temporal receptive fields [67, 70, 80], increase robustness to noise [81-83] and more specificity for processing natural sounds [12, 84]; but, it is also striking to see that in all those analyses as well as those that focused on single avian auditory cortical areas [85] there is a high degree of heterogeneity in the neural responses within each area. Here, we also found that neurons with high Categorical Information Indices could be found anatomically next to neurons with low

667 Categorical Information Indices. Some of this functional heterogeneity could be associated
668 with different cell types [69, 84] and a better understanding of the micro-circuitry in the avian
669 auditory cortical areas is needed [30]. It is interesting to note, however, that this mixing of
670 low level and high-level response properties is not unique to the avian auditory system as
671 similar heterogeneity has been found in the mouse [86] and ferret auditory cortex [87, 88].
672 Contrary to the visual system, the auditory system might preserve a higher mixture of low-
673 level and high-level sensory responses properties at multiple stages of processing including
674 the higher auditory areas involved in auditory object recognition. If this is true and
675 universally found in vertebrates, it might be a necessary property of the computations needed
676 for auditory object recognition, potentially related to the fact that complexity in auditory
677 signals is in time-varying spectral patterns that quickly disappear; the fleeting nature of
678 sounds could prevent higher processing stages from subsequently accessing lower-level
679 representations for additional information.

680

Methods

Animals and Stimuli

Four male and two female adult zebra finches (*Taeniopygia guttata*) were used for the electrophysiological experiments. The birds were bred and raised in family cages until they reached adulthood, and then maintained in uni-sex groups. Although birds could only freely interact with their cage-mates, all cages were in the same room allowing for visual and acoustical interactions between all birds in the colony. All birds were given seeds, water, grid and nest material ad libitum and were supplemented with eggs, lettuce and bath once a week. All animal procedures were approved by the Animal Care and Use Committee of the University of California Berkeley and were in accordance with the NIH guidelines regarding the care and use of animals for experimental procedures.

Vocalizations used as stimuli during neurophysiological experiments were recorded from 15 adult birds and 8 chicks (20-30 days old). The vocalization bank obtained contains 486 vocalizations that included for each bird most of the calls in the Zebra finch repertoire: 7 call-types in adults and 2 in chicks. The adult calls included the following affiliative calls: Song (So), Distance Call (DC), Tet call (Te) and Nest Call (Ne); and the following non-affiliative calls: Wsst or aggressive call (Ws), the Distress Call (Di) and one of the two alarm calls, the Thuk (Th). The juvenile calls included the Begging call (Be) and the Long Tonal Call (LT). Additional information about these stimuli and their behavioral meanings can be found in [39, 40, 89].

For the neurophysiological experiments, a new subset of the vocalization bank was used at each electrophysiological recording site. This subset was made from a representative number of vocalizations from the repertoire of individuals: three adult females, three adult males, two female chicks and two male chicks. From each individual caller, we randomly chose 3 call bouts from each category or fewer if fewer than 3 call bouts were obtained for

706 that particular call-type and individual. The maximum number of stimuli that could be
707 selected in that procedure was therefore 3x7x3 (adult males x repertoire x renditions) +
708 3x6x3 (adult females x repertoire x renditions) + 4x2x3 (juveniles x repertoire x renditions) =
709 141. Fewer stimuli were used when we had fewer renditions than 3 for a particular bird or
710 when the signal from a single unit was lost before the end of the recording. The average
711 number of stimuli played for each single unit was 114 (sd = 22, min = 34, max = 123). Ten
712 trials were acquired for each stimulus with a few exceptions (min=9, max = 11). Sounds
713 were broadcasted in a random order using an RX8 processor (TDT System III, sample
714 frequency 24414.0625 Hz) connected to a speaker (PCxt352, Blaupunkt, IL, USA) facing the
715 bird at approximately 40cm. The sound level was calibrated on song stimuli to obtain
716 playbacks at 75dB SPL measured at the bird's location using a sound meter (Digital Sound
717 Level Meter, RadioShack).

718 ## Neurophysiological and Histological Procedures.

719 Extra-cellular electrophysiological recordings were performed in 6 urethane
720 anesthetized adult zebra finches. The birds were placed in a sound-attenuated chamber
721 (Acoustic Systems, MSR West, Louisville, CO, USA) and sound presentation and neural
722 recording were performed using custom code written in TDT software language and TDT
723 hardware (TDT System III). Sounds were broadcasted in a random order as described above.
724 Neural responses were recorded using the signal of two (5 subjects) or one (1 subject) 16-
725 tungsten electrode arrays, band-pass filtered between 300Hz and 5kHz and collected by an
726 RZ5-2 processor (TDT System III, sample frequency 24414.0625 Hz). The electrode arrays
727 consisted of two rows of 8 electrodes with row separation of 500 mm and inter-electrode
728 separation within row of 250 mm. Electrode impedances were approximately 2 MOhms.
729 When two electrode arrays were used, they were placed each in one hemisphere. Spike
730 arrival times and spike shapes of multiple units were obtained by voltage threshold. The level

731 of the threshold was set automatically by the TDT software using the variance of the voltage
732 trace in absence of any stimuli. Electrodes were progressively lowered and neural responses
733 were collected as soon as auditory responses to song, white noise, Distance call or limited
734 modulation noise could be identified on half of the electrodes in each hemisphere (the stimuli
735 used to identify auditory neurons were different from the stimuli used in the analysis).
736 Several recording sites were randomly selected by progressively deepening the penetration of
737 the electrodes and ensuring at least 100 µm between two sites. On average 4.2±2 sites (mean
738 ± sd) were recorded per bird and per hemisphere at a depth ranging from 400 µm to 2550 µm.
739 After the last recording site, the subject was euthanized by overdose of isoflurane and
740 transcardially perfused. Coronal slices of 20µm obtained with a cryostat were then
741 alternatively stained with Nissl staining or simply mounted in Fluoroshield medium (F-6057,
742 Fluoroshield with DAPI, Sigma-Aldrich). While Fluoroshield slices were used to localize
743 electrode tracks, Nissl stained slices were used to identify the position of the 6 auditory areas
744 investigated here: the three regions of Field L (L1, L2 and L3), 2 regions of Mesopallium
745 Caudale (CM): Mesopallium Caudomediale (CMM) and Mesopallium Caudolaterale (CLM);
746 and Nidopallium Caudomediale (NCM). By aligning pictures, we were able to anatomically
747 localize most of the recording sites and calculate the approximate coordinates of these sites.
748 Since we could not localize the Y-sinus on slices, we used the position of the Lamina Pallio-
749 Subpallialis (LPS) peak as the reference point for the rostro-caudal axis in all subjects. The
750 surface of the brain and the midline were the reference for respectively the dorsal-ventral axis
751 and the medial-lateral axis. The approximate coordinates of units were used to build 3-D
752 reconstructions of all single unit positions in an hypothetic brain.
753 Single unit isolation was performed off-line using custom software that used a
754 combination of supervised and unsupervised clustering algorithms. These clustering
755 algorithms used the spike-snippets shape as described by a PCA. Sorted units where declared

to be single units based on spike shape reliability across snippets. The spike shape reliability measure was a signal to noise ratio (SNR) where the signal was the difference between the maximum and the minimum of the average snippet and the noise was the standard deviation of this measure across all snippets. Single units in our data set have an SNR > 5. Additional details on these experimental procedures can be found in [40].

Data Analysis: Time-varying Spike Rate Estimation

The data of neural responses from 404 out of 914 isolated single units were used in this study. The 404 were selected based on a prior analysis that showed that this subset of units were not only auditory but also contained information about call-types, in the sense that call-types could be decoded above chance level from neural responses (see [40]). Here, we analyzed the neural response in the first 600ms after stimulus onset.

For each stimulus, the 9 to 11 raw spike patterns of 600ms, sampled at 10kHz, were combined to obtain the corresponding time varying spike rate (sample frequency set at 1kHz) by applying a locally adaptive kernel bandwidth optimization method [41]. In cases where the neuron did not respond to any of the presentations of the stimulus or responded only once over all presentations, the rate was estimated as being constant for the 600ms duration of the neural response. For those two unresponsive cases, the rate was set to be 1/(2*Ntrials*NTimes) in the absence of any spike or 1/(Ntrials* NTimes) in case of one spike, with Ntrials the number of stimulus presentations (9-11) and NTimes the number of time points at which the rate was estimated (here 600, for a 600ms neural response section with a sampling rate set at 1kHz).

Calculations of cumulative information requires the estimation of very large distributions which sizes grow exponentially with the number of time points investigated. To investigate cumulative information values up to 600ms after stimulus onset, time-varying

781 rates were sampled at 10ms (Nyquist limit frequency of 50Hz). To estimate, the amount of
782 information potentially lost by this low-pass filtering, we estimated an information value
783 based on coherence analysis of the signal to noise ratio in the raw spike train. The coherence
784 between a single spike train (R) and the actual time-varying mean response (A) γ_{AR}^2 can be
785 derived from the coherence between the peristimulus time histogram (PSTH) obtained from
786 half of the trials and the PSTH obtained from the other half [90].

787 $$\gamma_{AR}^2 = \left[1 - \frac{M}{2} \times \left(1 - \sqrt{\frac{1}{\gamma^2_{\bar{R}_{1,M/2}\bar{R}_{2,M/2}}}}\right)\right]$$

788 where M the total number of trials (presentations of the stimuli) and $\gamma^2_{\bar{R}_{1,M/2}\bar{R}_{2,M/2}}$ the coherence
789 between the two PSTHs calculated on half of the trials. The coherence between two
790 responses is a function of frequency (ω). An estimate of the mutual information (in bits per
791 second) between R and A responses can then be obtained by integrating over all frequencies
792 [4, 90]:

793 $$I_{AR} = -\int_0^\infty \log_2\left[1 - \gamma_{AR}^2(\omega)\right] d\omega$$

794 For each unit, we estimated the percentage of information preserved as the ratio
795 between I_{AR} calculated up to 50Hz and I_{AR} calculated over all frequencies. Over all units,
796 96.7% ±6.9% (mean ± SD) of information was conserved by a lowpass filtering at 50Hz and
797 only 88 out of 404 cells had information losses greater than 5%. For each unit, we also
798 calculated the proportion of cumulative power across frequencies in the time varying spike
799 rate estimation obtained with the KDE before low-pass filtering and down-sampling
800 (averaged periodogram in overlapping 200 ms Hanning windows and 1 kHz sampling rate).
801 The cumulative sum of the power was calculated across frequencies and normalized by the
802 maximum power value to obtain the proportion of cumulative power. On average across

803 units, the cumulative power reached 98.8%±1.6% (mean ± SD) at 50Hz, further validating
804 our choice of the temporal resolution (Supp Fig. 1).
805
806 ## Information Theoretic Calculations.
807 As described in the results, the time-varying *instantaneous* mutual information
808 between the stimulus S and the response Y_t can be written as a difference in Shannon
809 entropies:
810 $$I_t = H(Y_t) - H(Y_t|S)$$
811 and the *cumulative* mutual information for neural responses that are discretized into time
812 intervals is given by: $CI_t = H(Y_t, Y_{t-1}, Y_{t-2}, \ldots, Y_0) - H(Y_t, Y_{t-1}, Y_{t-2}, \ldots, Y_0 | S)$
813 In the present paper we calculated 4 different types of information: the stimulus instantaneous
814 information, the categorical instantaneous information, the stimulus cumulative information
815 and the categorical cumulative information. Stimulus instantaneous and cumulative
816 information were calculated for all 404 units, while categorical instantaneous and cumulative
817 information were calculated on a restricted set of 337 neurons that presented at least one time
818 point with a significant value of stimulus cumulative information (significant threshold set as
819 3 times the local error, see below for error calculations). While we verified our assumptions
820 (minimal information loss with spike rate binning, Poisson distributions of spike counts and
821 maximum value of spike counts) on the full set of 404 units, the population analysis of time-
822 varying information presented in the results section only include the relevant dataset of 337
823 neurons.
824 The custom Matlab code used to calculate time-varying information values is available at
825 https://github.com/julieelie/PoissonTimeVaryingInfo along with a tutorial on how to use the
826 core functions.
827

The Instantaneous Information

The conditional response entropy and the response entropy are obtained from the distribution of the conditional probability of neural responses given the stimulus, $p(y_t|s)$, and the distribution of probability of each stimulus $p(s_i)$:

$$H(Y_t|S) = \sum_i p(s_i) \sum_{y_t=0}^{R_{Max}} - p(y_t \,|\, s_i) \log_2 p(y_t \,|\, s_i)$$

$$H(Y_t) = \sum_{y_t=0}^{R_{Max}} - p(y_t) \log_2 p(y_t)$$

$$\text{with } p(y_t) = \textstyle\sum_i p(s_i) p(y_t|s_i)$$

We modeled the distribution of neural responses to a given stimulus s_i as an inhomogeneous Poisson process. The conditional probability of response (spike count) given the stimulus is then:

$$p(y_t|s_i) = \frac{\mu_{s_i}(t)^{y_t}}{y_t!} e^{-\mu_{s_i}(t)}$$

And the local entropy is:

$$H(Y_t \,|\, s_i) = \mu_{s_i}(t)\left[1 - \log_2\left(\mu_{s_i}(t)\right)\right] + e^{-\mu_{s_i}(t)} \sum_{y_t=0}^{R_{Max}} \frac{\mu_{s_i}(t)^{y_t} \log_2 (y_t!)}{y_t!}$$

Because, in our data, the probability of response is very small for high values of y_t, calculations of entropies were bounded for y_t between zero and R_{Max}. Here we set $R_{Max} = 20$ which corresponds to a rate of 2 spike/ms in the 10 ms analysis windows. The maximum rate observed in all of our neurons across all time bins was 0.8 spike/ms (Sup. Fig. 2). Note that this very high firing rate (800 Hz) was only observed only once; that is in one 10 ms time windows across all neurons (404) and all stimuli (114*60= 6840) or with a p=1/ 2763360. This is clearly the very upper limit of a distribution with a long tail. Our time-varying rates

were well below that upper bound but we verified that the cumulative probability up to $R_{Max} = 20$ was numerically identical to 1 before estimating entropies. As described above (see time-varying spike rate estimation), we also enforced a lower bound for $\mu_{s_i}(t)$ of 1/20.

The total conditional entropy at time *t* is:

$$H(Y_t \mid S) = \sum_{i=1}^{n_s} \sum_{y_t=0}^{R_{Max}} -p(s_i)\left(p(y_t|s_i)\log_2 p(y_t|s_i)\right)$$

where $p(s_i)$ is the probability of observing stimulus s_i and $n_s$is the number of stimuli sampled: it is the average of the local entropies obtained for the conditional probability of response for each stimulus s_i. Assuming that our sample is representative of stimuli encountered, each stimulus is equally probable, $p(s_i) = \frac{1}{n_s}$ or:

$$H(Y_t \mid S) = \frac{1}{n_s}\sum_{i=1}^{n_s} H(Y_t \mid s_i)$$

Alternatively, one can assume that each call category is equally probable. If k_i is the number of stimuli in the particular call category *c* to which s_i belongs and n_c is the number of categories, then:

$$p(s_i) = \left(\frac{1}{k_i}\right)\left(\frac{1}{n_c}\right)$$

for $s_i \in c$. Then:

$$H(Y_t \mid S) = \frac{1}{n_c}\sum_{i=1}^{n_s} \frac{1}{k_i} H(Y_t \mid s_i)$$

The unconditional probability (i.e. across all stimuli) of a response at time t is not Poisson but is given by a weighted sum of Poisson with different mean rates:

$$p(y_t) = \sum_{i=1}^{n_s} p(s_i)p(y_t \mid s_i)$$

868 $$p(y_t) = \frac{1}{n_c}\sum_{i=1}^{n_s}\frac{1}{k_i}\left[\frac{\mu_{s_i}(t)^{y_t}}{y_t!}e^{-\mu_{s_i}(t)}\right]$$

869

870 The response entropy is obtained from these unconditional probabilities:

871 $$H(Y_t) = -\sum_{y_t=0}^{R_{Max}} p(y_t)\log_2\left(p(y_t)\right)$$

872 $$H(Y_t) = -\sum_{y_t=0}^{R_{Max}}\left[\frac{1}{n_c}\sum_{i=1}^{n_s}\frac{1}{k_i}\left[\frac{\mu_{s_i}(t)^{y_t}}{y_t!}e^{-\mu_{s_i}(t)}\right]\right]\log_2\left[\frac{1}{n_c}\sum_{i=1}^{n_s}\frac{1}{k_i}\left[\frac{\mu_{s_i}(t)^{y_t}}{y_t!}e^{-\mu_{s_i}(t)}\right]\right]$$

873

874 ## The Cumulative Information.

875 The conditional probability of a time varying response is the joint probability of

876 observing $(y_t, y_{t-1}, y_{t-2}, \ldots)$ given s_i. Given our Poisson assumption, the conditional

877 probability of response at t is independent of the conditional response at previous times.

878 $$p(y_t, y_{t-1}, y_{t-2}, \ldots \mid s_i) = p(y_t \mid s_i)p(y_{t-1} \mid s_i)p(y_{t-2} \mid s_i)\ldots$$

879 We can show that the conditional entropy of the joint responses is the sum of the individual

880 entropies:

881 $$H(Y_t, Y_{t-1}, Y_{t-2}, \ldots \mid S) = \frac{1}{n_c}\sum_{i=1}^{n_s}\frac{1}{k_i}\sum_{y_t=0}^{\infty}\sum_{y_{t-1}=0}^{\infty}\sum_{y_{t-2}=0}^{\infty}\ldots\left(p(y_t \mid s_i)p(y_{t-1} \mid s_i)p(y_{t-2} \mid s_i)\ldots \log_2\left\{p(y_t \mid s_i)p(y_{t-1} \mid s_i)p(y_{t-2} \mid s_i)\ldots\right\}\right)$$

882

883 $$H(Y_t, Y_{t-1}, Y_{t-2}, \ldots \mid S) = \frac{1}{n_c}\sum_{i=1}^{n_s}\frac{1}{k_i}\left\{\sum_{y_t=0}^{\infty}\left(p(y_t \mid s_i)\log_2 p(y_t \mid s_i)\right) + \sum_{y_{t-1}=0}^{\infty}\left(p(y_{t-1} \mid s_i)\log_2 p(y_{t-1} \mid s_i)\right) + \sum_{y_{t-2}=0}^{\infty}\left(p(y_{t-2} \mid s_i)\log_2 p(y_{t-2} \mid s_i)\right) + \ldots\right\}$$

884 $$H(Y_t, Y_{t-1}, Y_{t-2}, \ldots \mid S) = H(Y_t \mid S) + H(Y_{t-1} \mid S) + H(Y_{t-2} \mid S) + \ldots$$

885

886 The probability of the time varying response is the joint probability of observing

887 $(y_t, y_{t-1}, y_{t-2}, \ldots)$. This joint probability cannot be expressed as the product of the

888 probabilities at different times because these are not independent. The joint unconditional

889 probability distribution is:

890 $$p(y_t, y_{t-1}, y_{t-2}, \ldots) = \frac{1}{n_c}\sum_{i=1}^{n_s}\frac{1}{k_i}[p(y_t \mid s_i)p(y_{t-1} \mid s_i)p(y_{t-2} \mid s_i)\ldots] \neq p(y_t)p(y_{t-1})p(y_{t-2})\ldots$$

891 This joint probability distribution could be expressed as a product of probabilities by

892 assuming that most of the interdependence can be calculated from the previous time point, as

893 in the Markov chain assumption at a beginning of the time series at t=0. In all cases, the joint

894 probability distribution can be written as:

895 $$p(y_t, y_{t-1}, y_{t-2}, \ldots) = p(y_t|y_{t-1}, y_{t-2}, \ldots)p(y_{t-1}|y_{t-2}, y_{t-3}, \ldots)\ldots p(y_0)$$

896 or when it is approximated by a first-order Markov chain:

897 $$p(y_t, y_{t-1}, y_{t-2}, \ldots) \cong p(y_t|y_{t-1})p(y_{t-1}|y_{t-2})\ldots p(y_0)$$

898 The conditional probability of y_t given y_{t-1} is:

899 $$p(y_t|y_{t-1}) = \frac{p(y_t, y_{t-1})}{p(y_{t-1})}$$

900 $$p(y_t|y_{t-1}) = \frac{\frac{1}{n_c}\sum_{i=1}^{n_s}\frac{1}{k_i}[p(y_t \mid s_i)p(y_{t-1} \mid s_i)]}{\frac{1}{n_c}\sum_{i=1}^{n_s}\frac{1}{k_c}[p(y_{t-1} \mid s_i)]}$$

901

902 Note that this joint probability distribution can have very high dimensions. Assuming the

903 number of spikes $y_t \in [0,19]$, the number of probabilities that must be estimated is 20^{nt} where

904 *nt* is the number of windows in time. For example, calculating all the probability of all the

905 outcomes for 10 windows (100ms) requires 20^{10}~10^{13} calculations. On the other hand, the

Markov chain approximation only requires the estimation of all pair-wise joint probability distributions: for 10 windows and 20 outcomes, the number of calculations is $(10)(20^2)$~4000.

The response entropy is then calculated from the joint probability distribution:

$$H(Y_t,Y_{t-1},Y_{t-2},\ldots) = -\sum_{y_t=0}^{\infty}\sum_{y_{t-1}=0}^{\infty}\sum_{y_{t-2}=0}^{\infty}\ldots p(y_t,y_{t-1},y_{t-2},\ldots)\log p(y_t,y_{t-1},y_{t-2},\ldots)$$

To estimate this response entropy, we investigated various approaches: a time-running cumulative information, the Markov chain approximation and Monte Carlo with importance sampling. Monte Carlo with importance sampling gave the best results and was therefore used in our analyses. We briefly describe the three approaches. The time-running cumulative information consisted in calculating the full cumulative information (using all possible spike events) but only for a fixed number of successive time windows. We estimated that we could easily calculate all possible probabilities for 4 time-windows, corresponding to a 40 ms history. This approach gave the best estimate of the information in 40 ms windows but, in our system, grossly underestimated the cumulative information: some of the information in successive 40 ms is clearly independent (Sup. Fig. 3).

The second approximation was based on Markov chain of variable orders up to 4 (also 40 ms). With this approximation, we overestimated the cumulative information: the correlation time of the time-varying rates for different stimuli is clearly also greater than 40 ms. Using the first order Markov chain approximation:

$$\begin{aligned} &H(Y_t,Y_{t-1},Y_{t-2},\ldots) \\ &\quad = -\sum_{y_t}\sum_{y_{t-1}}\ldots \\ &\quad \sum_{y_0}\{p(y_t\,|\,y_{t-1})p(y_{t-1}\,|\,y_{t-2})\ldots p(y_0)\log\left(p(y_t\,|\,y_{t-1})p(y_{t-1}\,|\,y_{t-2})\ldots p(y_0)\right)\} \end{aligned}$$

927
$$=-\sum_{y_t}\sum_{y_{t-1}}\dots\sum_{y_0}\{(p(y_t\,|\,y_{t-1})p(y_{t-1}\,|\,y_{t-2})\dots p(y_0))$$
$$(\log(p(y_t\,|\,y_{t-1}))+\log p(y_{t-1}\,|\,y_{t-2})+\dots+\log p(y_0))\}$$

928

929 Expanding that sum, the last term is:

930 $L.T.=-\sum_{y_t}\sum_{y_{t-1}}\dots\sum_{y_0}\{(p(y_t\,|\,y_{t-1})p(y_{t-1}\,|\,y_{t-2})\dots p(y_0))\log(p(y_0)\}$

931
$$=-\sum_{y_0}\sum_{y_1}\dots\left\{\sum_{y_t}p(y_t|y_{t-1})\right\}(p(y_{t-1}\,|\,y_{t-2})\dots p(y_0))\log(p(y_0)$$

932
$$=-\sum_{y_0}\sum_{y_1}\dots\left\{\sum_{y_{t-1}}p(y_{t-1}|y_{t-2})\right\}(p(y_{t-2}\,|\,y_{t-3})\dots p(y_0))\log(p(y_0)$$

933
$$\dots$$

934
$$=-\sum_{y_0}\left\{\sum_{y_1}p(y_1|y_0)\right\}p(y_0)\log(p(y_0)$$

935
$$=-\sum_{y_0}p(y_0)\log(p(y_0)$$

936
$$=H(Y_0)$$

937

938 The second to last term is:

939
$$=-\sum_{y_0}\sum_{y_1}\dots\left\{\sum_{y_t}p(y_t|y_{t-1})\right\}(p(y_{t-1}\,|\,y_{t-2})\dots p(y_0))\log(p(y_1|y_0))$$

940
$$=-\sum_{y_0}p(y_0)\sum_{y_1}p(y_1\,|\,y_0)\log p(y_1|y_0)$$

941
$$=H(Y_1|Y_0)$$

942

943 The third to last term is:

944
$$=-\sum_{y_0}\sum_{y_1}\dots\left\{\sum_{y_t}p(y_t|y_{t-1})\right\}\{(p(y_{t-1}\,|\,y_{t-2})\dots p(y_0))(\log(p(y_2|y_1))\}$$

945 $$=-\sum_{y_0}\sum_{y_1}\sum_{y_2}\{(p(y_2\,|\,y_1)p(y_1|y_0)p(y_0)(\log\,(p(y_2|y_1))\}$$

946 $$=-\sum_{y_1}\sum_{y_2}\left\{\left(p(y_2\,|\,y_1)\sum_{y_0}\{p(y_1|y_0)p(y_0)\}\right)\log\,(p(y_2|y_1)\right\}$$

947 $$=-\sum_{y_1}\sum_{y_2}(p(y_2\,|\,y_1)p(y_1)\log\,(p(y_2|y_1)$$

948 $$=-\sum_{y_1}p(y_1)\sum_{y_2}p(y_2\,|\,y_1)\log\,(p(y_2|y_1))$$

949

950

951 $$=H(Y_2|Y_1)$$

952

953 and, similarly, for all the other terms.

954 Thus, the response entropy using the Markov chain approximation is:

955 $$H(Y_t,Y_{t-1},Y_{t-2},\ldots)=H(Y_t\,|\,Y_{t-1})+H(Y_{t-1}\,|\,Y_{t-2})+\ldots+H(Y_0)$$

956 with $H(Y_t\,|\,Y_{t-1})=-\sum_{y_{t-1}}[p(y_{t-1})\sum_{y_t}p(y_t|y_{t-1})\log_2\,(p(y_t|y_{t-1}))]$

957 This approximation can be extended using estimates at two previous time points, *etc.*:

958 $$\begin{aligned}&H(Y_t,Y_{t-1},Y_{t-2},\ldots)\\&=H(Y_t\,|\,Y_{t-1},Y_{t-2})+H(Y_{t-1}\,|\,Y_{t-2},Y_{t-3})+\ldots+H(Y_2\,|\,Y_1,Y_0)+\;H(Y_1|Y_0)\\&+H(Y_0)\end{aligned}$$

959 where the conditional probability based on two prior measurements is:

960 $$p(y_t|y_{t-1},y_{t-2})=\frac{p(y_t,y_{t-1},y_{t-2})}{p(y_{t-1},y_{t-2})}$$

961 $$p(y_t|y_{t-1},y_{t-2})=\frac{\frac{1}{n_c}\sum_{i=1}^{n_s}\frac{1}{i_c}[p(y_t\,|\,s_i)p(y_{t-1}\,|\,s_i)p(y_{t-2}\,|\,s_i)]}{\frac{1}{n_c}\sum_{i=1}^{n_s}\frac{1}{i_c}[p(y_{t-1}\,|\,s_i)p(y_{t-2}\,|\,s_i)]}$$

where $H(Y_t \mid Y_{t-1},Y_{t-2}) = -\sum_{y_{t-1}}$

$$\sum_{y_{t-2}}[p(y_{t-1},y_{t-2})\sum_{y_t}p(y_t|y_{t-1},y_{t-2})\log_2\left(p(y_t|y_{t-1},y_{t-2})\right)$$

Finally, we estimated cumulative information using Monte Carlo with importance sampling. In Monte Carlo in conjunction with importance sampling, N_i samples or, here, time varying responses $\vec{y}_i$, are taken from a proposal distribution, $q(\vec{y})$. The actual probability, $p(\vec{y}_i)$, is calculated exactly at those samples and an estimate of the expected value of the measure of interest (here $f(\vec{y}) = \log\left(p(\vec{y})\right)$) is obtained by the average of $f(\vec{y})$ at the sample points, $\vec{y}_i$, weighted by the likelihood ratio *p/q*:

$$E[f(\vec{y})] = \frac{1}{N_i}\sum_i \left(p(\vec{y}_i)/q(\vec{y}_i)\right)f(\vec{y}_i)$$

Our proposal distribution was based on the distribution at each time point and assuming independence across time:

$$q(y_t,y_{t-1},y_{t-2},\ldots) = p(y_t)p(y_{t-1})p(y_{t-2})\ldots$$

For each sample obtained from the proposal distribution q we calculated the actual probability value using:

$$p(y_t,y_{t-1},y_{t-2},\ldots) = \frac{1}{n_c}\sum_{i=1}^{n_s}\frac{1}{k_i}[p(y_t \mid s_i)p(y_{t-1} \mid s_i)p(y_{t-2} \mid s_i)\ldots]$$

and used that probability value in the estimation of the entropy. Monte Carlo samples were chunked in groups of 100,000 samples and at each additional sample chunk, a bootstrapped/jackknife bias corrected mean and standard error were estimated (see below). Sampling stopped when the standard error was below 0.2 bits or at a max number of samples set to 5,000,000 samples. If the error at the maximum number of samples was greater than 0.6 bits, the estimation was deemed unreliable and the calculation was not performed for any successive time points.

Bias Correction and Standard Error for Information Calculations.

The small number of trials used to estimate spike rates is the source of bias and uncertainty in our calculation of information: a small number of stimulus presentations increase the probability of obtaining by chance estimated spike rate that are different between stimuli and so yields a positive bias on information calculations. We used a Jackknife procedure on the estimation of spike rate for each stimulus to correct for this positive bias. Jackknife kernel density estimate of the rate were obtained by applying the locally adaptive kernel bandwidth optimization method on the Ntrials possible sets of Ntrials-1 spike patterns of each stimulus (Ntrials being the number of stimulus presentation of a given stimulus). Moreover, uncertainty about information values comes from the sampling errors on spike rate and on the Monte Carlo estimation of joint spike rate probability distributions (cumulative information only). These errors on information calculations were estimated by bootstrapping the jackknife procedure:

$Error = \sqrt[2]{\frac{\sum_{NB} var(I_{JN})}{NB}}$ with NB the number of boostrap ($NB = 20$), I_{JN} the bias-corrected estimation of information obtained from the Jackknife procedure.

Calculation of the Expected Value of Categorical Information Given the Stimulus Information

We computed a Categorical Information Index (CII) that compared the empirical categorical cumulative information for call-type categories, CCI, to three hypothetical values: a floor (CCI_{Floor}) , an expected value (CCI_{Exp}) and a ceiling value (CCI_{Ceil}). The floor value is the categorical cumulative information obtained from random categories. The expected value is the categorical cumulative information that would be achieved if the stimulus information

1009 was 1) equally distributed for each stimulus and 2) could be used for classifying stimuli into
1010 groups. Note that the second assumption is not necessarily true in the actual data because the
1011 categorical information is based on averaging the probabilities for stimulus from the same
1012 category and thus effectively averaging time-varying rates. If time-varying rates are not
1013 grouped by categories, then it is possible that two stimuli from two different categories are
1014 distinguishable based on their time-varying rate, but that, the average time-varying rates for
1015 the two categories are not distinguishable, or less so than expected from the average pair-wise
1016 distances. The ceiling value corresponds to the case where all the cumulative information
1017 about stimuli is used for the categorization and none to discriminate stimuli belonging to the
1018 same category: CCI_{Ceil}. The CII is a number between 0 and 2 that is then calculated as:

1019 $$CII = \frac{CCI - CCI_{Floor}}{CCI_{Exp} - CCI_{Floor}} \; if \; CCI < CCI_{Exp}$$

1020 $$CII = 1 + \frac{CCI - CCI_{Exp}}{CCI_{Ceil} - CCI_{Exp}} \; if \; CCI \geq CCI_{Exp}$$

1021

1022 The following three steps were taken to calculate the expected categorical information
1023 (CCI_{Exp}) from the stimulus cumulative information. First, the stimulus mutual information,
1024 *mi*, was expressed as the conditional probability of correct stimulus decoding, *p,* for any
1025 given stimulus (and assumed to be equal for all stimuli). Given a confusion matrix of size *n*x*n*
1026 obtained from a decoder for *n* stimuli, with *p* as the conditional probability given a stimulus
1027 of correct decoding (diagonal terms) and thus *(1-p)/(n-1)* as the conditional probability of
1028 error (off-diagonal terms), the mutual information is equal to:

1029 $$mi = p\left[2\log p - \log\frac{p}{n}\right] + (1-p)\left[2\log\frac{1-p}{n-1} - \log\frac{1-p}{(n-1)n}\right]$$

1030 The above equation was inverted numerically to solve for *p* given *mi*. Second, a new
1031 matrix was generated by grouping rows and columns of joint probabilities (and not
1032 conditional) to form a confusion matrix for categories. The number of stimulus in each

category was matched to the actual values in the neurophysiological data on a unit per unit basis. Third, the expected mutual information for categories was then estimated from this new confusion matrix by subtracting the total entropy obtain from the joint probabilities, from the sum of the entropies of the marginal distributions for the rows and columns:

$$mi_{cat} = H_{Row} + H_{Col} - H_{Tot}$$

Data availability

The custom Matlab code used to calculate time varying information values is available at https://github.com/julieelie/PoissonTimeVaryingInfo, along with a tutorial on modeled data.

Acknowledgement

This research used the Savio computational cluster resource provided by the Berkeley Research Computing program at the University of California, Berkeley (supported by the UC Berkeley Chancellor, Vice Chancellor for Research, and Chief Information Officer).

References

1. Shannon CE, Weaver W. The matematical theory of communication. Chicago: University of Illinois Press; 1963.
2. Wu MCK, David SV, Gallant JL. Complete functional characterization of sensory neurons by system identification. Annual Review of Neuroscience. Annual Review of Neuroscience. 292006. p. 477-505.
3. Rieke F, Warland D, de Ruyter van Steveninck R, Bialek W. Spikes: Exploring the Neural Code. Cambridge, MA: MIT Press; 1997.
4. Borst A, Theunissen FE. Information theory and neural coding. Nat Neurosci. 1999;2(11):947-57. doi: 10.1038/14731. PubMed PMID: 10526332.
5. Rolls ET, Treves A. The neuronal encoding of information in the brain. Progress in Neurobiology. 2011;95(3):448-90. doi: 10.1016/j.pneurobio.2011.08.002. PubMed PMID: WOS:000297614000009.
6. Stone JV. Principles of Neural Information Theory: Sebtel Press; 2018. 197 p.
7. Optican LM, Richmond BJ. Temporal encoding of two-dimensional patterns by single units in primate inferior temporal cortex. III. Information theoretic analysis. Journal of Neurophysiology. 1987;57:162-78.
8. Reinagel P, Reid RC. Temporal coding of visual information in the thalamus. J Neurosci. 2000;20(14):5392-400. PubMed PMID: 10884324.
9. Brenner N, Strong SP, Koberle R, Bialek W, de Ruyter van Steveninck RR. Synergy in a neural code. Neural Comput. 2000;12(7):1531-52. PubMed PMID: 10935917.
10. Chechik G, Anderson M, Baryosef O, Young E, Tishby N, Nelken I. Reduction of Information Redundancy in the Ascending Auditory Pathway. Neuron. 2006;51(3):359-68. doi: 10.1016/j.neuron.2006.06.030.
11. Rieke F, Bodnar DA, Bialek W. Naturalistic stimuli increase the rate and efficiency of information transmission by primary auditory afferents. Proc R Soc Lond B Biol Sci. 1995;262(1365):259-65.
12. Hsu A, Woolley SM, Fremouw TE, Theunissen FE. Modulation power and phase spectrum of natural sounds enhance neural encoding performed by single auditory neurons. J Neurosci. 2004;24(41):9201-11. Epub 2004/10/16. doi: 10.1523/JNEUROSCI.2449-04.2004. PubMed PMID: 15483139.
13. Amin N, Gastpar M, Theunissen FE. Selective and efficient neural coding of communication signals depends on early acoustic and social environment. PLoS One. 2013;8(4):e61417. Epub 2013/05/01. doi: 10.1371/journal.pone.0061417. PubMed PMID: 23630587; PubMed Central PMCID: PMC3632581.
14. Atick J. Could information theory provide an ecological theory of sensory processing? Network. 1992;3:213-51.
15. Strong SP, Koberle R, de Ruyter van Steveninck R, Bialek W. Entropy and information in neural spike trains. Phys Rev Letters. 1998;80(1):197-200.
16. Kanwisher N, Yovel G. The fusiform face area: a cortical region specialized for the perception of faces. Philosophical Transactions of the Royal Society B-Biological Sciences. 2006;361(1476):2109-28. doi: 10.1098/rstb.2006.1934. PubMed PMID: WOS:000242685500005.
17. DeWitt I, Rauschecker JP. Phoneme and word recognition in the auditory ventral stream. Proceedings of the National Academy of Sciences of the United States of America.

2012;109(8):E505-E14. doi: 10.1073/pnas.1113427109. PubMed PMID: WOS:000300495100008.

18. Kuboki R, Sugase-Miyamoto Y, Matsumoto N, Richmond BJ, Shidara M. Information Accumulation over Time in Monkey Inferior Temporal Cortex Neurons Explains Pattern Recognition Reaction Time under Visual Noise. Frontiers in Integrative Neuroscience. 2017;10. doi: 10.3389/fnint.2016.00043. PubMed PMID: WOS:000391870900001.

19. Bair W, Cavanaugh JR, Smith MA, Movshon JA. The timing of response onset and offset in macaque visual neurons. Journal of Neuroscience. 2002;22(8):3189-205. PubMed PMID: WOS:000174841300021.

20. Bisley JW, Krishna BS, Goldberg ME. A rapid and precise on-response in posterior parietal cortex. Journal of Neuroscience. 2004;24(8):1833-8. doi: 10.1523/jneurosci.5007-03.2004. PubMed PMID: WOS:000189210300005.

21. Wang X, Lu T, Snider RK, Liang L. Sustained firing in auditory cortex evoked by preferred stimuli. Nature. 2005;435(7040):341-6.

22. Zheng Y, Escabi MA. Distinct Roles for Onset and Sustained Activity in the Neuronal Code for Temporal Periodicity and Acoustic Envelope Shape. Journal of Neuroscience. 2008;28(52):14230-44. doi: 10.1523/jneurosci.2882-08.2008.

23. Victor JD, Purpura KP. Nature and precision of temporal coding in visual cortex: A metric-space analysis. Journal of Neurophysiology. 1996;76(2):1310-26. PubMed PMID: WOS:A1996VD97200050.

24. Mechler F, Victor JD, Purpura KP, Shapley R. Robust temporal coding of contrast by V1 neurons for transient but not for steady-state stimuli. Journal of Neuroscience. 1998;18(16):6583-98. PubMed PMID: WOS:000075246500046.

25. Delorme A, Thorpe SJ. Face identification using one spike per neuron: resistance to image degradations. Neural Networks. 2001;14(6-7):795-803. doi: 10.1016/s0893-6080(01)00049-1. PubMed PMID: WOS:000171417300018.

26. Heil P. First-spike latency of auditory neurons revisited. Current Opinion in Neurobiology. 2004;14(4):461-7. doi: 10.1016/j.conb.2004.07.002.

27. Johansson RS, Birznieks I. First spikes in ensembles of human tactile afferents code complex spatial fingertip events. Nature Neuroscience. 2004;7(2):170-7. doi: 10.1038/nn1177. PubMed PMID: WOS:000188468500015.

28. Rolls ET, Franco L, Aggelopoulos NC, Jerez JM. Information in the first spike, the order of spikes, and the number of spikes provided by neurons in the inferior temporal visual cortex. Vision Research. 2006;46(25):4193-205. doi: https://doi.org/10.1016/j.visres.2006.07.026.

29. de Heer WA, Huth AG, Griffiths TL, Gallant JL, Theunissen FE. The Hierarchical Cortical Organization of Human Speech Processing. Journal of Neuroscience. 2017;37(27):6539-57. doi: 10.1523/jneurosci.3267-16.2017. PubMed PMID: WOS:000404758300013.

30. Tsunada J, Cohen YE. Neural mechanisms of auditory categorization: from across brain areas to within local microcircuits. Front Neurosci. 2014;8:161. doi: 10.3389/fnins.2014.00161. PubMed PMID: 24987324; PubMed Central PMCID: PMC4060728.

31. Sharpee TO, Atencio CA, Schreiner CE. Hierarchical representations in the auditory cortex. Current Opinion in Neurobiology. 2011;21(5):761-7. PubMed PMID: WOS:000298121400014.

32. Gifford GW, 3rd, MacLean KA, Hauser MD, Cohen YE. The neurophysiology of functionally meaningful categories: macaque ventrolateral prefrontal cortex plays a critical

role in spontaneous categorization of species-specific vocalizations. J Cogn Neurosci. 2005;17(9):1471-82.
33. Grimsley JM, Shanbhag SJ, Palmer AR, Wallace MN. Processing of communication calls in Guinea pig auditory cortex. PLoS One. 2012;7(12):e51646. Epub 2012/12/20. doi: 10.1371/journal.pone.0051646. PubMed PMID: 23251604; PubMed Central PMCID: PMC3520958.
34. Plakke B, Diltz MD, Romanski LM. Coding of vocalizations by single neurons in ventrolateral prefrontal cortex. Hear Res. 2013;305:135-43. doi: 10.1016/j.heares.2013.07.011. PubMed PMID: 23895874; PubMed Central PMCID: PMC3979279.
35. Miller CT, Thomas AW, Nummela SU, de la Mothe LA. Responses of primate frontal cortex neurons during natural vocal communication. Journal of Neurophysiology. 2015;114(2):1158-71. doi: 10.1152/jn.01003.2014. PubMed PMID: WOS:000360554100038.
36. Carruthers IM, Natan RG, Geffen MN. Encoding of ultrasonic vocalizations in the auditory cortex. J Neurophysiol. 2013;109(7):1912-27. Epub 2013/01/18. doi: 10.1152/jn.00483.2012. PubMed PMID: 23324323.
37. Comins JA, Gentner TQ. Perceptual categories enable pattern generalization in songbirds. Cognition. 2013;128(2):113-8. doi: 10.1016/j.cognition.2013.03.014. PubMed PMID: 23669049; PubMed Central PMCID: PMC3684258.
38. Ter Maat A, Trost L, Sagunsky H, Seltmann S, Gahr M. Zebra finch mates use their forebrain song system in unlearned call communication. PLoS One. 2014;9(10):e109334. doi: 10.1371/journal.pone.0109334. PubMed PMID: 25313846; PubMed Central PMCID: PMC4196903.
39. Elie JE, Theunissen FE. The vocal repertoire of the domesticated zebra finch: a data-driven approach to decipher the information-bearing acoustic features of communication signals. Animal cognition. 2016;19(2):285-315. doi: 10.1007/s10071-015-0933-6. PubMed PMID: WOS:000370170300004.
40. Elie JE, Theunissen FE. Meaning in the avian auditory cortex: neural representation of communication calls. The European journal of neuroscience. 2015;41(5):546-67. doi: 10.1111/ejn.12812. PubMed PMID: MEDLINE:25728175; PubMed Central PMCID: PMC25728175.
41. Shimazaki H, Shinomoto S. Kernel bandwidth optimization in spike rate estimation. J Comput Neurosci. 2010;29(1-2):171-82. doi: 10.1007/s10827-009-0180-4. PubMed PMID: 19655238; PubMed Central PMCID: PMCPMC2940025.
42. Panzeri S, Treves A. Analytical estimates of limited sampling biases in different information measures. Network: Computation in Neural Systems. 1996;7:87-107.
43. Fortune ES, Margoliash D. Cytoarchitectonic organization and morphology of cells of the field L complex in male zebra finches (Taenopygia guttata). J Comp Neurol. 1992;325(3):388-404.
44. Vates GE, Broome BM, Mello CV, Nottebohm F. Auditory pathways of caudal telencephalon and their relation to the song system of adult male zebra finches (Taenopygia guttata). J Comp Neurol. 1996;366:613-42.
45. Wang Y, Brzozowska-Prechtl A, Karten HJ. Laminar and columnar auditory cortex in avian brain. Proceedings of the National Academy of Sciences. 2010;107(28):12676-81. doi: 10.1073/pnas.1006645107.
46. Elliott TM, Theunissen FE. The Avian Auditory Pallium. Auditory Cortex2011. p. 429-42.

47. Brown EN, Barbieri R, Ventura V, Kass RE, Frank LM. The time-rescaling theorem and its application to neural spike train data analysis. Neural Computation. 2002;14(2):325-46. doi: 10.1162/08997660252741149. PubMed PMID: WOS:000173321400003.
48. Kass RE, Ventura V, Brown EN. Statistical issues in the analysis of neuronal data. Journal of Neurophysiology. 2005;94(1):8-25. doi: 10.1152/jn.00648.2004. PubMed PMID: WOS:000230135500004.
49. Victor JD, Purpura KP. Spike Metrics. In: Grun S, Rotter S, editors. Analysis of Parallel Spike Trains. Springer Series in Computational Neuroscience. 7. New York: Springer; 2010. p. 129-56.
50. Franco L, Rolls ET, Aggelopoulos NC, Treves A. The use of decoding to analyze the contribution to the information of the correlations between the firing of simultaneously recorded neurons. Exp Brain Res. 2004;155(3):370-84. doi: 10.1007/s00221-003-1737-5. PubMed PMID: WOS:000220026100012.
51. Quian Quiroga R, Panzeri S. Extracting information from neuronal populations: information theory and decoding approaches. Nat Rev Neurosci. 2009;10(3):173-85. doi: 10.1038/nrn2578. PubMed PMID: 19229240.
52. DeWeese MR, Wehr M, Zador AM. Binary spiking in auditory cortex. Journal of Neuroscience. 2003;23(21):7940-9. PubMed PMID: WOS:000185001700027.
53. Hamilton LS, Edwards E, Chang EF. A Spatial Map of Onset and Sustained Responses to Speech in the Human Superior Temporal Gyrus. Current Biology. 2018. doi: 10.1016/j.cub.2018.04.033.
54. Nelken I, Rotman Y, Bar Yosef O. Responses of auditory-cortex neurons to structural features of natural sounds. Nature. 1999;397(6715):154-7.
55. Lewicki MS. Efficient coding of natural sounds. Nat Neurosci. 2002;5(4):356-63. PubMed PMID: 11896400.
56. Woolley SM, Fremouw TE, Hsu A, Theunissen FE. Tuning for spectro-temporal modulations as a mechanism for auditory discrimination of natural sounds. Nat Neurosci. 2005;8(10):1371-9.
57. Rodriguez FA, Chen C, Read HL, Escabi MA. Neural modulation tuning characteristics scale to efficiently encode natural sound statistics. J Neurosci. 2010;30(47):15969-80. Epub 2010/11/26. doi: 10.1523/JNEUROSCI.0966-10.2010. PubMed PMID: 21106835; PubMed Central PMCID: PMC3351116.
58. Santoro R, Moerel M, De Martino F, Goebel R, Ugurbil K, Yacoub E, et al. Encoding of Natural Sounds at Multiple Spectral and Temporal Resolutions in the Human Auditory Cortex. Plos Computational Biology. 2014;10(1):14. doi: 10.1371/journal.pcbi.1003412. PubMed PMID: WOS:000337948500014.
59. Theunissen FE, Elie JE. Neural processing of natural sounds. Nat Rev Neurosci. 2014;15(6):355-66. doi: 10.1038/nrn3731. PubMed PMID: 24840800; PubMed Central PMCID: PMC24840800.
60. Heil P, Irvine DRF. The posterior field P of cat auditory cortex: Coding of envelope transients. Cerebral Cortex. 1998;8(2):125-41. doi: 10.1093/cercor/8.2.125. PubMed PMID: WOS:000072118300004.
61. Liang L, Lu T, Wang X. Neural representations of sinusoidal amplitude and frequency modulations in the primary auditory cortex of awake primates. J Neurophysiol. 2002;87(5):2237-61. PubMed PMID: 11976364.
62. Furukawa S, Middlebrooks JC. Cortical representation of auditory space: information-bearing features of spike patterns. J Neurophysiol. 2002;87(4):1749-62. PubMed PMID: 11929896.
63. Mouterde SC, Elie JE, Mathevon N, Theunissen FE. Single Neurons in the Avian Auditory Cortex Encode Individual Identity and Propagation Distance in Naturally Degraded

Communication Calls. Journal of Neuroscience. 2017;37(13):3491-510. doi: 10.1523/jneurosci.2220-16.2017. PubMed PMID: WOS:000397823700007.
64. Town SM, Wood KC, Bizley JK. Sound identity is represented robustly in auditory cortex during perceptual constancy. Nature communications. 2018;9(1):4786. doi: 10.1038/s41467-018-07237-3.
65. VanRullen R, Guyonneau R, Thorpe SJ. Spike times make sense. Trends in Neurosciences. 2005;28(1):1-4. doi: 10.1016/j.tins.2004.10.010. PubMed PMID: WOS:000226682200001.
66. Theunissen F, Miller JP. Temporal encoding in nervous systems: a rigorous definition. J Comput Neurosci. 1995;2(2):149-62. Epub 1995/06/01. PubMed PMID: 8521284.
67. Sen K, Theunissen FE, Doupe AJ. Feature analysis of natural sounds in the songbird auditory forebrain. J Neurophysiol. 2001;86(3):1445-58. Epub 2001/09/06. PubMed PMID: 11535690.
68. Woolley SM, Gill PR, Fremouw T, Theunissen FE. Functional groups in the avian auditory system. J Neurosci. 2009;29(9):2780-93. PubMed PMID: 19261874.
69. Nagel K, Doupe A. Organizing Principles of Spectro-Temporal Encoding in the Avian Primary Auditory Area Field L. Neuron. 2008;58(6):938-55. doi: 10.1016/j.neuron.2008.04.028.
70. Kim G, Doupe A. Organized Representation of Spectrotemporal Features in Songbird Auditory Forebrain. Journal of Neuroscience. 2011;31(47):16977-90. PubMed PMID: WOS:000297586900010.
71. Chew SJ, Mello C, Nottebohm F, Jarvis E, Vicario DS. Decrements in auditory responses to a repeated conspecific song are long-lasting and require two periods of protein synthesis in the songbird forebrain. Proc Natl Acad Sci U S A. 1995;92(8):3406-10.
72. Nagel KI, Doupe AJ. Temporal Processing and Adaptation in the Songbird Auditory Forebrain. Neuron. 2006;51(6):845-59. doi: 10.1016/j.neuron.2006.08.030.
73. Bee MA, Micheyl C, Oxenham AJ, Klump GM. Neural adaptation to tone sequences in the songbird forebrain: patterns, determinants, and relation to the build-up of auditory streaming. J Comp Physiol A -Neuroethol Sens Neural Behav Physiol. 2010;196(8):543-57. PubMed PMID: WOS:000280240000003.
74. Rieke F, Yamada W, Moortgat K, Lewis ER, Bialek W. Real time coding of complex sounds in the auditory cortex. Advances in Biosciences. 1992;83:315-22.
75. Shamma S. On the role of space and time in auditory processing. Trends in Cognitive Sciences. 2001;5(8):340-8.
76. Lu T, Wang X. Information content of auditory cortical responses to time-varying acoustic stimuli. J Neurophysiol. 2004;91(1):301-13. Epub 2003 Oct 1.
77. David SV, Shamma SA. Integration over Multiple Timescales in Primary Auditory Cortex. Journal of Neuroscience. 2013;33(49):19154-66. PubMed PMID: WOS:000328110100012.
78. Osman AF, Lee CM, Escabi MA, Read HL. A Hierarchy of Time Scales for Discriminating and Classifying the Temporal Shape of Sound in Three Auditory Cortical Fields. Journal of Neuroscience. 2018;38(31):6967-82. doi: 10.1523/jneurosci.2871-17.2018. PubMed PMID: WOS:000440551400013.
79. Ma SW, Ter Maat A, Gahr M. Power-law scaling of calling dynamics in zebra finches. Scientific reports. 2017;7:11. doi: 10.1038/s41598-017-08389-w. PubMed PMID: WOS:000408103900005.
80. Kozlov AS, Gentner TQ. Central auditory neurons have composite receptive fields. Proceedings of the National Academy of Sciences of the United States of America.

1289 2016;113(5):1441-6. doi: 10.1073/pnas.1506903113. PubMed PMID:
1290 WOS:000369085100087.
1291 81. Moore RC, Lee T, Theunissen FE. Noise-invariant Neurons in the Avian Auditory
1292 Cortex: Hearing the Song in Noise. Plos Computational Biology. 2013;9(3). PubMed PMID:
1293 WOS:000316864200015; PubMed Central PMCID: PMC23505354
1294 82. Schneider DM, Woolley SMN. Sparse and Background-Invariant Coding of
1295 Vocalizations in Auditory Scenes. Neuron. 2013;79(1):141-52. PubMed PMID:
1296 WOS:000321802000015.
1297 83. Carruthers IM, Laplagne DA, Jaegle A, Briguglio JJ, Mwilambwe-Tshilobo L, Natan
1298 RG, et al. Emergence of invariant representation of vocalizations in the auditory cortex.
1299 Journal of Neurophysiology. 2015;114(5):2726-40. doi: 10.1152/jn.00095.2015. PubMed
1300 PMID: WOS:000367436400018.
1301 84. Meliza CD, Margoliash D. Emergence of selectivity and tolerance in the avian
1302 auditory cortex. J Neurosci. 2012;32(43):15158-68. Epub 2012/10/27. doi:
1303 10.1523/JNEUROSCI.0845-12.2012. PubMed PMID: 23100437; PubMed Central PMCID:
1304 PMC3498467.
1305 85. Billimoria CP, Kraus BJ, Narayan R, Maddox RK, Sen K. Invariance and sensitivity
1306 to intensity in neural discrimination of natural sounds. Journal of Neuroscience.
1307 2008;28(25):6304-8. PubMed PMID: ISI:000256890000003.
1308 86. Rothschild G, Nelken I, Mizrahi A. Functional organization and population dynamics
1309 in the mouse primary auditory cortex. Nature Neuroscience. 2010;13(3):353-U21. doi:
1310 10.1038/nn.2484. PubMed PMID: WOS:000274860100018.
1311 87. Bizley JK, Walker KM, Silverman BW, King AJ, Schnupp JW. Interdependent
1312 encoding of pitch, timbre, and spatial location in auditory cortex. J Neurosci.
1313 2009;29(7):2064-75. PubMed PMID: 19228960.
1314 88. Walker KMM, Bizley JK, King AJ, Schnupp JWH. Multiplexed and Robust
1315 Representations of Sound Features in Auditory Cortex. Journal of Neuroscience.
1316 2011;31(41):14565-76. PubMed PMID: WOS:000296019600014.
1317 89. Zann R. The Zebra Finch: A Synthesis of Field and Laboratory Studies. Oxford:
1318 Oxford University Press; 1996.
1319 90. Hsu A, Borst A, Theunissen FE. Quantifying variability in neural responses and its
1320 application for the validation of model predictions. Network. 2004;15(2):91-109. Epub
1321 2004/06/25. PubMed PMID: 15214701.
1322

1323

Supplemental Figures

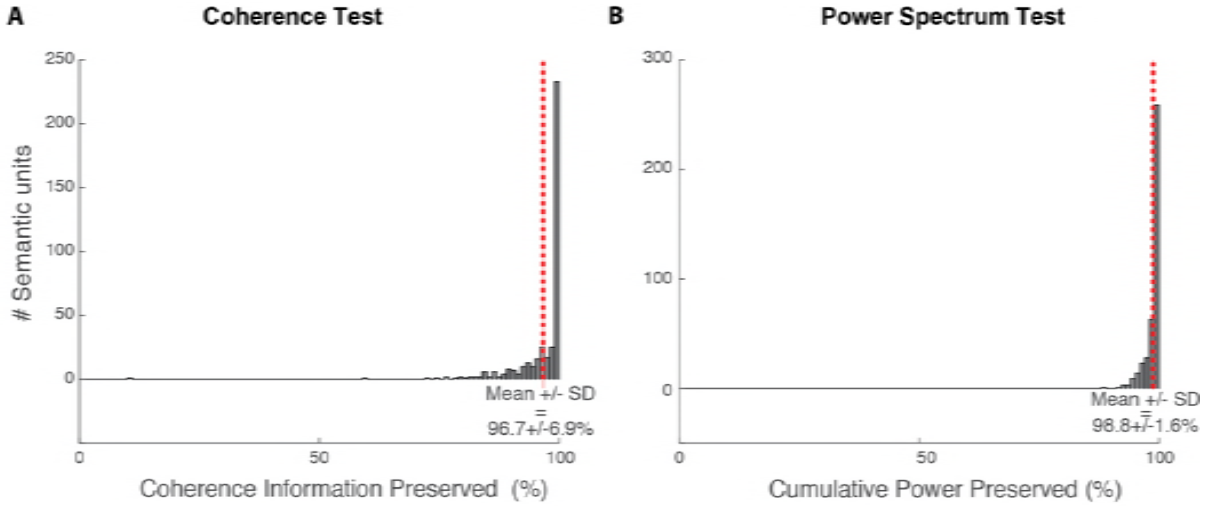

Supplemental Figure 1. Tests for Temporal Resolution. We performed two tests to assess the potential information loss from sampling the time-varying rate at 50 Hz (10 ms bins). **A.** The Coherence Test is based on the coherence between individual spike trains. A measure of total coherence (Information Coherence) can be obtained by integrating over frequencies (see Methods). The Information Coherence obtained by integrating from 0 to 50 Hz can then be compared to the Information Coherence obtained for the entire frequency range of 0 to 500 Hz. The histogram shows the number of cells versus the fraction of Information Coherence in 0-50 Hz. **B.** The Power Spectrum Test is based on the power spectrum of the time-varying rates for each neuron obtained with the Kernel Density estimation (sample frequency: 1kHz). Just as for the Coherence Information, the fraction of the power between 0-50 Hz relative to the power between 0-500 Hz was estimated for all cells. The histogram shows the number of neurons as a function of that fraction.

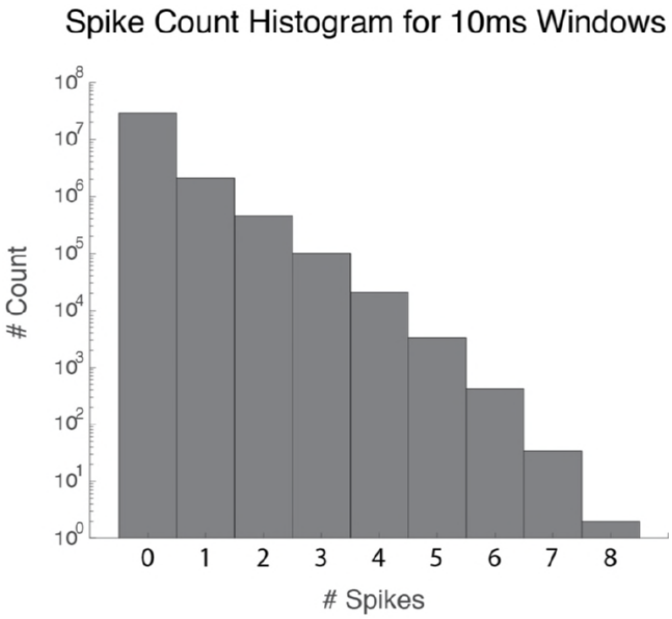

Supplemental Figure 2. Distribution of Spike Counts in 10 ms Bins. This distribution is shown as the number of time bins across all 404 neurons, all stimuli and all time points that had 0, 1, … 8 spikes. Not a single neuron had more than 8 spikes in a 10 ms bins andhigh spiking events were very rare (only one 10ms bin with 8 spikes over all neurons, all time bins and all stimuli). The average number of spikes per 10 ms bin was 0.108 .

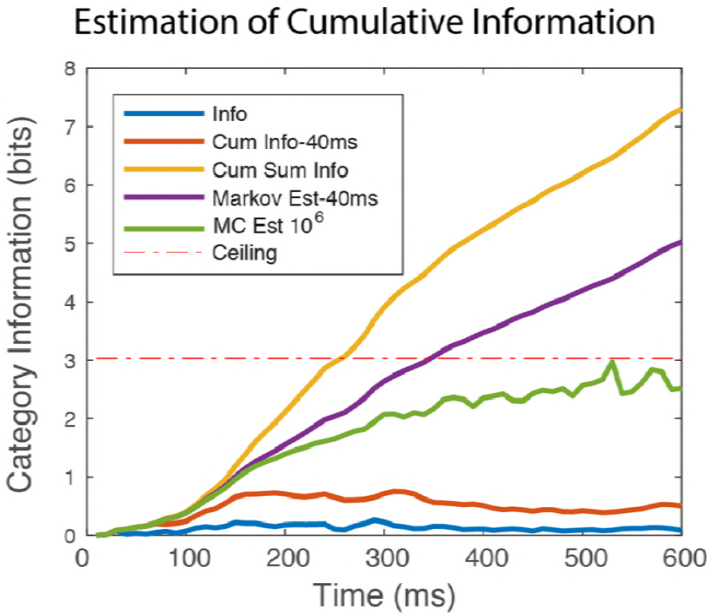

Supplemental Figure 3. Estimation of the Cumulative Information. Three methods were tested for the estimation of the Cumulative Information (see Methods): a Markov chain approximation of variable order up to 4 or 40 ms (purple line), the exact information in 4 bins (40 ms) evaluated in running windows (red line), and a Monte Carlo estimation (green line). For comparison, the instantaneous time-varying information in 10 ms windows (blue line) and the integral of that information (yellow line) are also shown. The ceiling value corresponds here to the $\log_2(N_{cat}=9)$ because this example is showing the categorical cumulative information of the neuron. The Markov chain overestimates the cumulative information while the running window of 40 ms underestimates the cumulative information. The information values plotted here were obtained from the neural data of Example Neuron 1 shown in Fig. 3 and also in Sup. Fig. 4. This high-firing, high-information neuron allowed us to verify that the calculations were correct around ceiling values.

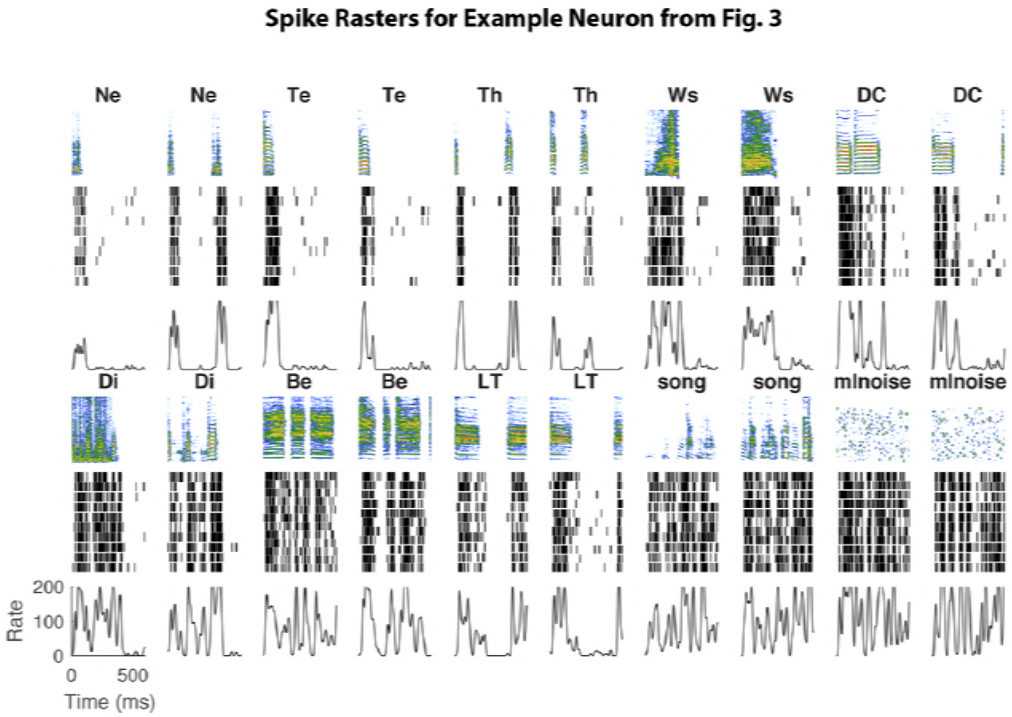

Supplemental Figure 4. Example Spike Rasters for Example Neuron 1. The spectrogram of two (randomly chosen) stimuli from each stimulus category are shown with the corresponding spike rasters for 10 trials and a smoothed PSTH for the example neuron shown in Fig. 3. This neuron had a very high stimulus driven firing rate and responded to all sound stimuli. The mlnoise stimulus is modulation limited noise: white noise that is low-pass filtered in amplitude and spectral modulations. This stimulus was used here to search for auditory regions but the responses to these synthetic sounds were not included in these analyses.

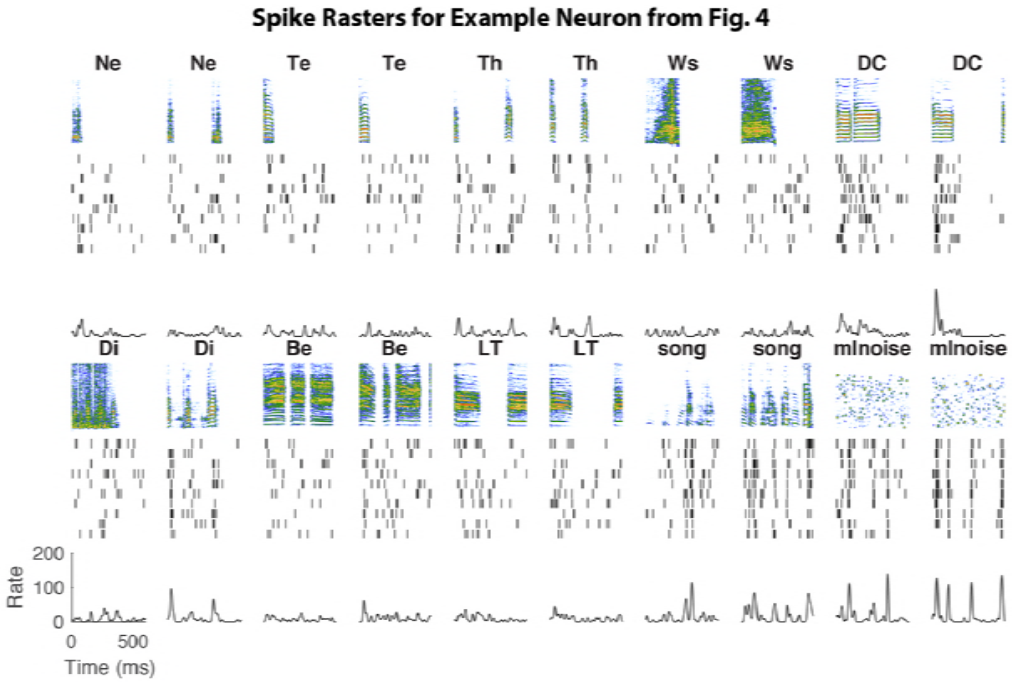

Supplemental Figure 5. Example Spike Rasters for Example Neuron 2. As Sup. Fig. 4 but for the Example Neuron 2. Example Neuron 2 also shown in Fig. 4 of the main paper is selective for Distance Calls (DC).

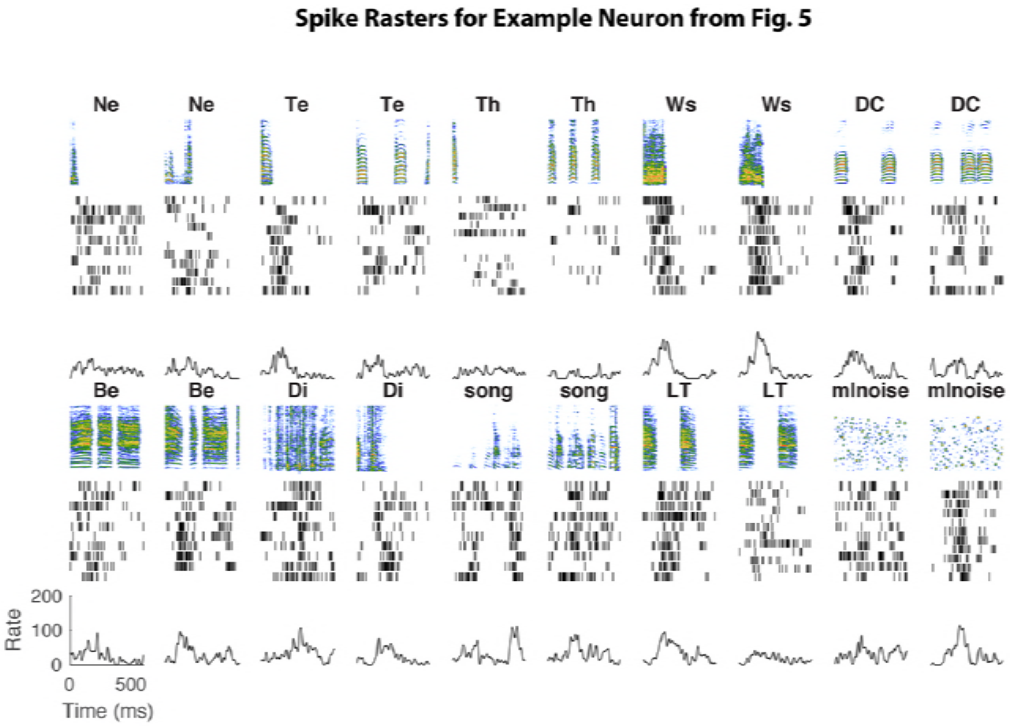

1377

1378 **Supplemental Figure 6. Example Spike Rasters for Example Neuron 3.** As Sup. Fig. 4
1379 but for the Example Neuron 3. Example Neuron 3 also shown in Fig. 5 of the main paper is
1380 selective for aggressive calls or Wsst Calls (Ws).
1381

1382

1383

1384